National Technical University of Athens

J.P.P.S. Computational Mechanics

Master Thesis

Numerical Study on a Metal Hydride Hydrogen Compressor

Konstantinos Deligiannis

Supervisor: Prof. Andreas Boudouvis

Acknowledgements

I would like to express my sincere gratitude and appreciation to Professor Andreas Boudouvis and Professor Athanasios Stubos, my research supervisors, for their guidance and support during my master thesis work. I would also like to thank As. Professor Michalis Kavousanakis for his suggestions on improvements of this research work.

I am particularly grateful for the assistance provided by NCSR Demokritos staff, supporting me with all the required technical equipment to carry out my research work.

Finally, I would to offer special thanks to Hystore Technologies for making available the experimental data that were used in this work.

Abstract

The growing global energy demand and increasing concerns about environmental pollution have made hydrogen a realistic alternative option to the traditional fossil fuels. One of the key elements on the hydrogen supply chain is high-pressure hydrogen compression systems and further research and development is required for reaching technological maturity while moving towards a large-scale hydrogen economy. Metal hydride hydrogen compressors (MHC) is a promising technology for compression of hydrogen due to their heat driven operation, absence of moving parts, compactness, safety and reliability, and the potential to utilize waste heat instead of electricity for much, if not all, of the thermal requirements of the MH containers. This study aims to numerically investigate and predict the operating characteristics of a 6-stage MHC by modeling the energy and mass transfer phenomena that take place during absorption and desorption processes upon compression cycle.

A numerical time dependent model of the coupled dehydrogenation and hydrogenation process that predicts the operating conditions of the 6-stage MHC was achieved through Finite Element Analysis on Comsol Multyphysics software. Through this, the most crucial performance parameters of the 6-stage MHC were investigated. The hydrogenation/dehydrogenation fraction of metal hydrides, the transient pressure and temperature conditions and other performance characteristics such as cycle period, initial and final operation pressures of each stage were investigated and compared with experimental data. Key parameters that affect the accuracy of the results like material characteristics of Enthalpy, Entropy, Activation energy and reaction kinetic constants were highlighted and suggestions for further improvements on the numerical model were analyzed.

Keywords: hydrogen, compression, metal hydrides, numerical investigation, energy and mass transfer

Contents

1. Introduction

Hydrogen as an energy carrier

The growing global energy demand and increasing concerns about environmental pollution have made hydrogen a realistic alternative to the traditional fossil fuels. The world's energy consumption is expected to double over the next half century so significant changes in producing, distributing, storing and using energy are necessary (1). Hydrogen can be the ideal solution to all these issues. Hydrogen is the most abundant element in the universe and thus a never-ending and renewable source of energy. Furthermore, hydrogen can be produced from renewable and sustainable resources, such as biomass, solar and wind energies with no impact for the environment, thus offering a promising eco-friendly solution for the energy transition expected in the next decades.

Despite such advantages, two main issues prevent the generalized use of hydrogen as an efficient fuel, and with this, the energy transition towards an effective fossil-free solution. Firstly, hydrogen is an energy vector which means it is necessary to produce it before use, so energy is needed to synthesize hydrogen (2). Secondly, hydrogen exhibits the lowest volumetric energy density among the commonly used fuels, 0.01079 MJ/L at standard temperature and pressure which is much lower than that of petrol −34 MJ/L (3). Several methods have been developed to attempt to increase this value: (i) compression in gas cylinders; (ii) liquefaction in cryogenic tanks; (iii) storage in metal hydride alloys; (iv) adsorption onto large specific surface area-materials and (v) chemical storage in covalent and ionic compounds (formic acid, borohydride, ammonia) (4). Among these, compression is the most widely used method to store hydrogen although not the cheapest (5).

2. Hydrogen Compression

A summary of the most classical hydrogen compression technologies used for both stationary and automotive applications involving hydrogen as a renewable fuel are described below. An analysis of most common mechanical compressors, i.e., reciprocating, diaphragm, linear and ionic liquid compressors, as well as of innovative non-mechanical technologies specifically conceived for hydrogen applications, such as cryogenic, metal hydride, electrochemical and adsorption compressors is presented. The technical and design features, the basic operating principles and the level of performances potentially achievable for each single compressor technology are analyzed, emphasizing both their advantages and drawbacks.

2.1 Mechanical compressors

Mechanical compressors are the most widespread type of compressors used nowadays and are based on the direct conversion of mechanical energy into gas energy. There are several design approaches but positive displacement type compressors are mainly used for hydrogen compression. These work by reducing the confined volume in which hydrogen is contained by the use of a piston thus resulting in a higher gas pressure.

2.1.1 Reciprocating piston compressors

Basically, a single-stage reciprocating compressor consists of a piston-cylinder system, equipped with two automatic valves – one for intake and one for delivery (Fig 1). The piston is linked to a crankshaft by a connecting rod, converting the rotary motion of the moving units into the almost linear motion of the piston. This movement is known as reciprocating motion (6). The energy necessary for the compression is provided by either an electrical or a thermal machine. The piston movement towards the upper side of the cylinder, i.e., the Top Dead Centre (TDC), creates a partial vacuum in the lower part of the cylinder itself, opening the intake valve and allowing the gas to enter. The consequent suction phase lasts until the piston reaches the Bottom Dead Centre (BDC), then the intake valve is closed. Moving again towards the TDC, the gas is compressed until the pressure reaches the desired level, then the delivery valve is opened to discharge the gas. Reciprocating compressors produce high-pressure hydrogen especially when a multistage configuration is used (7). A first compression stage increases the hydrogen pressure up to a couple of atmospheres, before reaching the target value through the next stages. Currently, this configuration is particularly preferred in on-site hydrogen refueling stations where hydrogen is generated at a pressure around 0.6 MPa.

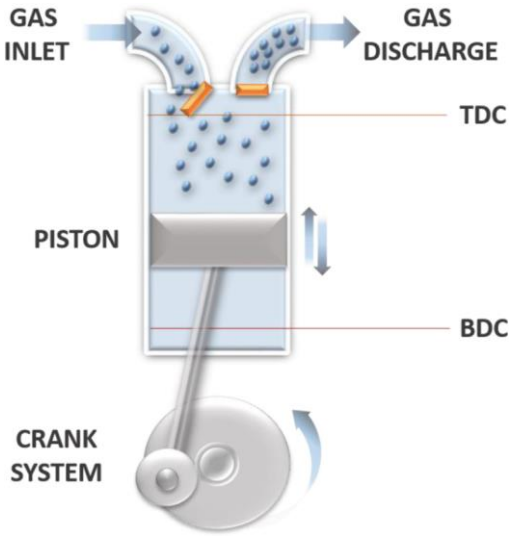

Figure 1: A reciprocating piston compressor

Although reciprocating compressors are widely used for applications involving hydrogen, several limitations mean they are not perfectly appropriate for this purpose. Firstly, the presence of several moving parts increases the cost because of the manufacturing complexity and difficulty in carrying out effective maintenance (8). Moreover, this type of compressor prevents the efficient cooling of hydrogen during compression because of the presence of moving parts, like the piston. This leads to an increase in the heat produced and makes it more difficult to manage thermal transfers (9). In addition, the back and forth movement of the piston causes pressure fluctuations inside the compression chamber, which can be detrimental since these may cause vibrations, noises and even lead to explosions. This of course reduces the system life of the overall hydrogen plant (10). Finally, embrittlement phenomena are one of the most important drawbacks in hydrogen reciprocating compressors which makes it necessary to carefully select the material used especially for the liner coating used for the protection of the walls (11).

Nonetheless, it should be noted that reciprocating compressors achieve very good performance levels especially when the multi-stage configuration is used because of the high value of the discharge pressure reached and their flexibility in size and capacity. Several improvements have been achieved in their design, like the upgrading to non-metallic ring and valves materials, the use of a tungsten carbide piston rod coating, and the implementation of continuous monitoring systems to predict possible failures (12). However, the aforementioned drawbacks attract interest for other devices aimed at compressing hydrogen more efficiently.

2.1.2 Diaphragm compressors

Thanks to their high throughput, lower power consumption and low cooling requirements, diaphragm compressors have proved highly effective for hydrogen applications (13). Generally, they are suitable when highly chemically pure gases have to be handled, since the direct contact between the gas and the piston is prevented (14). In fact, the gas is completely isolated from the piston, since its movement is transmitted to a hydraulic fluid, which in turn transmits the motion to a thin metal membrane called “diaphragm”, isolating hydrogen from the hydraulic part. The movement of the diaphragm into the cavity space, in which the gas is confined, reduces the available volume, thereby increasing gas pressure (Fig 2).

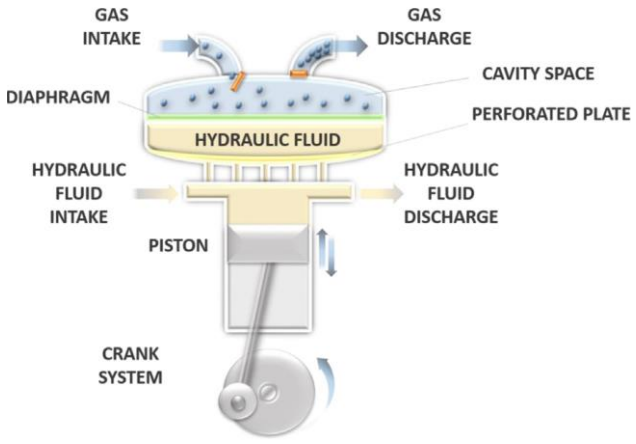

Figure 2: A metal diaphragm compressor

The diaphragm is actually made up of three different plates: (i) the process plate, on the hydrogen side which exclusively comes into contact with it; (ii) the hydraulic plate, on the hydraulic fluid side and (iii) the middle plate, set between the former two plates to detect possible leaks and avoid the diaphragm's failure. The hydraulic fluid in a diaphragm compressor is essentially oil. In reciprocating compressors oil could be used exclusively for lubricating purposes but in the diaphragm typology it directly controls the diaphragm movement. A specific hydraulic circuit provides oil to the hydraulic space, and is equipped with a hydraulic pressure limiter monitoring the pressure level beneath the diaphragm. A perforated plate acts as oil distributor, in order to achieve a uniform pressure load on the diaphragm plates (15).

Diaphragm compressors act properly to minimize the hydrogen leakages, since the hydrogen circuit is a closed loop which is well separated from the oil circuit so that the purity of the gas is always kept very high. This feature is crucial because hydrogen leakages affecting the mechanical compressors are the primary risk factor in hydrogen refueling stations. Diaphragm compressors are able to reach very high levels of volumetric efficiency which is a beneficial advantage for energy saving (16). However, one of the most important drawbacks of these compressors is their durability as they are weakened by mechanical stresses during operation. Since too high flow rates can cause the early failure of the diaphragm, a good design needs to include concavities and grooves ensuring proper flow distributions (17). Diaphragm compressors are especially appropriate for applications requiring low flow rates also because of the limited volume of the compression chambers commonly used (18). Diaphragm failure can be also caused by radial stresses related to the diaphragm deflection and strictly correlated to the geometry of the cavity space in which it moves. Further stresses can arise from the contact between the diaphragm and the perforated plate, causing fractures on the edge of the diaphragm and compromising the overall compressor operation.

2.1.3. Linear compressors

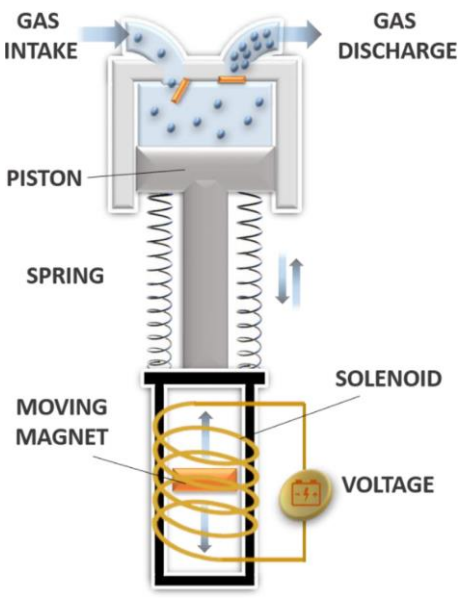

Figure 3: A linear compressor

Linear compressors are particularly used in cryogenic applications driven by Stirling cycle coolers and involving hydrogen and helium gas, as well as for domestic refrigeration (19). Compared to the former mechanical compressors, the piston is directly connected to a linear motor coupled with a resonating spring system (Fig 3), reducing the number of moving units because of the absence of a rod-crank assembly. The low number of rotating components makes the arrangement of the whole system simpler with regards to the compressors mentioned above thus leading to significant cost savings (20). Nevertheless, for stationary, industrial and automotive applications, there are no references about the use of linear compressors for hydrogen applications as these have only been considered an innovative way to compress hydrogen for a few years (21). The linear motors commonly used for driving the piston are magnetic-type and more specifically moving-coil and moving-magnet types. The Oxford moving-coil linear motor has been used for a long time, especially in aerospace applications, because of its high efficiency, low vibration, low noise emissions and long operation life (22).

A clear advantage in using linear compressors is that the piston and the cylinder are separated by a gas bearing system (23). This consists of driving an established amount of high-pressure gas back into the compression chamber with the gas acting as a pad to avoid friction. Moreover, this is beneficial for hydrogen applications since no oil lubes are used and the resultant discharge gas exhibits a high level of purity. In addition, this allows linear compressors to generate less than half the dB level of reciprocating compressors resulting in very silent operations (24).

2.1.4. Liquid compressors

Liquid compressors are particularly suitable for hydrogen applications. They are positive displacement devices using liquids to directly compress a gas working in the absence of mechanical sliding seals (25). They are widely recognized as achieving inexpensive compression because they are able to ensure a quasi-isothermal process (26). In fact, the liquid and the gas are compressed together but, since the liquid has a higher density and a higher heat capacity, the heat generated by compression is efficiently absorbed by the liquid and by the surrounding walls of the compression chamber. In addition, the resultant thermal management through the liquid itself means external heat exchangers do not need to be used thus reducing the cost of the overall system. As a result, this type of compression has a significant advantage over the other mechanical compressors in terms of efficiency with values higher than 83% (27).

2.1.4.1. Liquid piston compressors

Like in all other types of mechanical compressors, hydrogen confined in a closed space is directly compressed by a moving piston and in these devices it is liquid (28). More specifically, a column of liquid moves forth and back in a cylinder, compressing the gas introduced into its head. The liquid movement is driven by a pump which is connected to two cylinders in most applications and a compression step continually follows an expansion step (Fig 4). Liquid piston compressors are especially used in the context of compressed air energy storage in which electrical power is converted into compressed air energy at 20–30 MPa and which can be used on-site to power generators and turbines or can be stored for being used later. This kind of solution is usually associated with renewable energy plants (29).

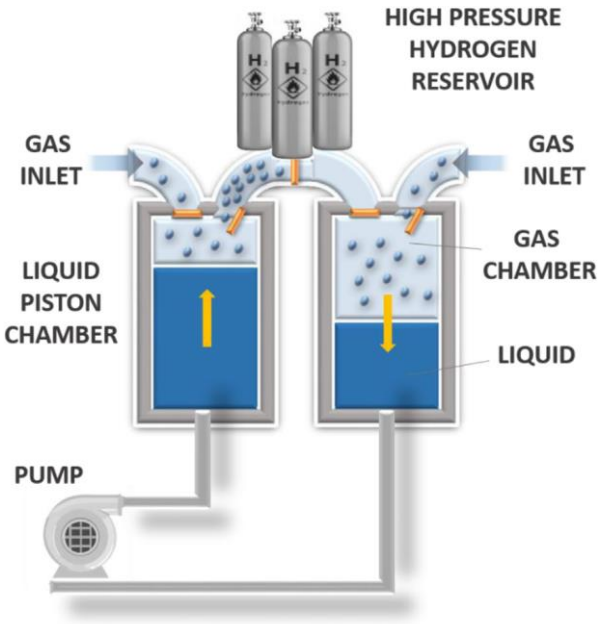

Figure 4: A liquid piston compressor

2.1.4.2. Liquid rotary compressors

Liquid rotary compressors are particularly used to compress a gas with a high liquid content (30). This design features an impeller located eccentrically in a stator frame and made up of a series of blades extending radially from it (Fig. 5). The impeller forces the liquid to move in an oscillatory manner overall, forming a ring compressing the gas introduced from a door placed in the rotor center (31). This kind of compressor particularly suits applications involving a vacuum or when saturated gases have to be handled (32). However, they are not widely used because of their low overall efficiency of about 50%.

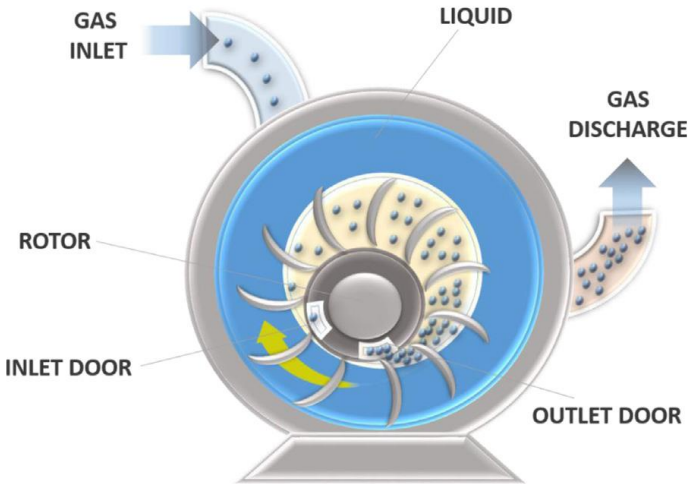

Figure 5: A liquid rotary compressor

2.1.4.2. Ionic liquid compressors

Ionic liquid compressors were specifically developed to increase compression efficiency when hydrogen is used. Ionic liquids are low-melting point salts and are therefore in the molten state at room temperature (33). They exhibit good thermal and chemical stability, high ionic conductivity, fire retardance, moderate viscosity, high polarity, negligible volatility and have no negative effects on human health while also offering low compressibility and superior lubricating abilities especially for high-pressure applications (34). They are interesting for a broad range of energy applications such as in batteries, fuel cells, solar cells and thermal storage. When used for compression applications, substituting the solid piston in a positive displacement device as well as in rotary configurations enables ionic liquids to achieve very good performances. This is thanks to their intrinsically low vapour pressure, their excellent low friction characteristics and the very low solubility of most gases into them. Specifically, hydrogen solubility in many ionic liquids is negligibly low which means very high volumetric efficiencies and high compression ratios can be achieved (35).

Ionic liquid compressors used in hydrogen fuelling stations have been proved to be a high-performance solution for the enhancement of the hydrogen value chain (36). The use of ionic liquids for hydrogen compression also ensures low energy consumption, long service life, low material costs and low noise

emission. Nevertheless, the risk of corrosion remains high, causing a decrease in overall efficiency by reducing the strength of the constituent materials and increasing the possibility of contamination by the corrosion products. Also, increased maintenance costs are to be expected.

Ionic liquids compressors for hydrogen applications have particularly been developed by the German international company Linde (36). Linde ionic compressors need only eight moving units to ensure good performances. This is clearly less than in reciprocating compressors which in turn reduces mechanical losses and improves overall efficiency. Hydrogen is compressed up to 90 MPa in only five steps and the good lubricant and coolant properties of the ionic liquids increase efficiency. It is noteworthy that no lube oils are used so that hydrogen is not polluted which is a great advantage especially in fuel cell applications.

2.2 Non-mechanical compressors

Even though mechanical compressors have been widely used for hydrogen applications, the low specific volumetric energy density affecting hydrogen in the gaseous state requires significant amounts of energy to compress enough gas. The actual compression work carried out by a mechanical hydrogen compressor is almost one-third of the amount of energy stored in the resultant compressed gas (37). Moreover, the efficiency of a mechanical hydrogen compressor is still modest in low-power applications (38). A possible solution might be storing hydrogen at cryogenic temperatures since the volumetric energy density is higher but the high cost and difficult thermal management mean this method is reserved for special applications only. Thermally-driven compressors have also proved themselves to be a good alternative as well as electrochemical compressors.

2.2.1. Cryogenic compression

Cryo-compression combines hydrogen liquefaction and compression with the benefits and challenges of both storage methods. It relies on the achievement of high pressures at very low temperatures. High pressure hydrogen is obtained by using cryogenic pumps able to reach a discharge pressure as high as 85 MPa, a hydrogen flow rate of 100 kg/h and a hydrogen density up to 80 g/L. Hence, instead of compressing hydrogen in the gaseous state, liquid hydrogen is pressurized and stored in cryo-compression systems consisting of a pressure vessel integrated in an insulated jacket to significantly reduce heat transfers between cold hydrogen and the exterior environment (39). The design of such hydrogen-compressing systems is very sophisticated and consists of several sequentially-arranged modular elements – a tank storing liquid hydrogen at low pressure, a cryogenic pump and cryo-compressed vessels. Liquid hydrogen is fed into a cryogenic pump through vacuum-insulated piping and then the cryo-pump brings liquid hydrogen to the desired pressure value. Vaporisers can be used downstream of the cryogenic pump in order to obtain high-pressure gaseous hydrogen (40), as shown in Fig. 6.

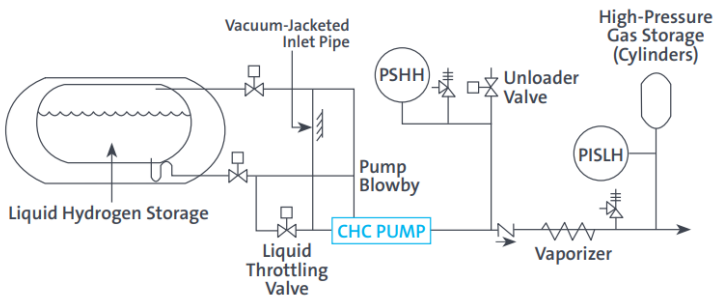

Figure 6: Basic components of a cryogenic compressor

A cryo-compressed hydrogen vessel fuelled by liquid hydrogen at high pressure offers several advantages when compared to the traditional cryogenic tanks storing liquid hydrogen at ambient pressure, such as (i) lower evaporative losses due to short periods of inactivity or low driving distances and (ii) smaller ullage spaces (up to 20%) to prevent danger (41). This solution enables 2–3 times more fuel to be stored than conventional ambient- temperature compressed vessels, i.e., a lower pressure is necessary to store a given amount of hydrogen. Hydrogen cryo-compression systems have more than twice the volumetric efficiency of a mechanical system (42).

Despite the aforementioned advantages of hydrogen cryo-compression over traditional compression, it is well known that the energy cost necessary to liquefy hydrogen is a definite drawback since only 30% of the chemical energy is stored, based on the hydrogen lower heating value (LHV) (43). Another important drawback hindering the use of cryo-compressed vessels, especially in automotive applications, is that they are not yet able to ensure a 10 year-long vacuum stability (44).

2.2.2. Electrochemical compressors

An electrochemical hydrogen compressor, also known as “electrochemical hydrogen pump”, is an innovative device that can be used to compress hydrogen with high recovery ratios of up to 95% and in applications requiring low gas quantities at very high pressures (45). It is based on the same basic principles as those of a proton-exchange membrane fuel cell (PEMFC). Low-pressure hydrogen is fed into the anode of an electrochemical cell where it splits into protons and electrons. The protons flow electrochemically through a solid polymer electrolyte while the electrons follow an external path, which is the electrical circuit controlled by the potential differential supplied to the system. Once the protons and electrons reach the cathode, they recombine to form hydrogen molecules again with a resultant increased pressure, as it shown in Figure 7. The discharge pressure depends entirely on the electrical voltage supplied to the system: the higher the voltage, the higher the pressure at which protons are reduced at the cathode.

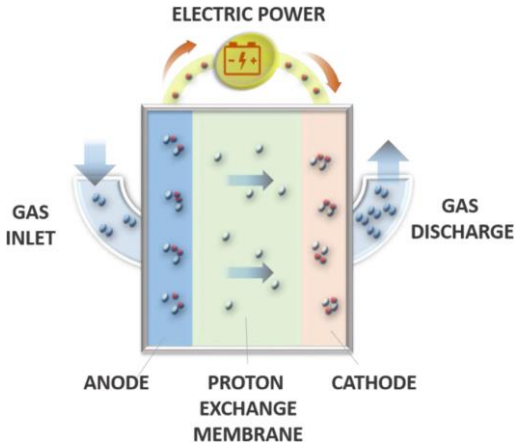

Figure 7: An Electrochemical compressor

In order to reach the pressure level required for many hydrogen applications, a cascade of multiple single cells can be used. It has been proved that very high pressures up to 85.7 MPa can be reached with a multi-

stack configuration. The HyET company has also demonstrated that it is possible to reach 100 MPa with the same operating principles (46). Moreover, in applications in which small hydrogen flow rates are required, an efficiency equal to 90% is potentially achievable. The multi-stack solution seems to be more advantageous than a multistage mechanical compressor – an electrochemical device is able to reach the same pressure level as a mechanical one using fewer stages, with no noise produced and a simpler design (47). Moreover, electrochemical compressors have been found to be more efficient than mechanical compressors. 7 kWh/ kg are necessary to compress hydrogen up to 20 MPa using a mechanical compressor but only 2 kWh/kg are needed with an electrochemical compressor (48).

In general, hydrogen electrochemical compressors exhibit a high level of efficiency when the discharge pressure is moderate. Therefore, even if several studies have found that this kind of system is potentially able to reach pressures up to 100 MPa, it is not convenient from practical and energetic standpoints. The use of hydrogen electrochemical compressors was shown to be a good and efficient solution when combined with other compressor systems like metal hydride or mechanical compressors (49). This was foreseen by the PHAEDRUS project which aimed to create a commercial hydrogen refueling station featuring a hybrid hydrogen compression system. Furthermore, as electrochemical compressors also require lower energy consumption at lower pressure range, they can be used at the outlet of an electrolyser to produce hydrogen at very high pressure thus enhancing the efficiency of the whole system. It is also worth highlighting that one the most important advantages of an electrochemical compressor is that it ensures vibration-free operation with no moving parts. Finally, if hydrogen is mixed with other gas, e.g. nitrogen or carbon dioxide, the hydrogen compressor is able to work even as a purifying device, producing high-purity hydrogen flows (50).

2.2.3. Adsorption compressors

A new emerging technology for hydrogen compression is based on adsorption and proceeds by means of changes in the system temperature, without any mechanical moving unit. A hydrogen adsorption compressor (Fig. 8) can be described as a thermodynamic engine in which compression is controlled by heat transfers between the compression reservoir and the system environment. Low-pressure hydrogen is fed into a closed tank filled with a solid bed consisting of a porous material with a high surface area and thus high adsorption potential. At specific temperature and pressure conditions, adsorption takes place exclusively on the surface of the porous material. After adsorption, heat is supplied to the system, resulting in an increase of temperature that produces hydrogen desorption. As a direct consequence, the density of the hydrogen bulk phase increases and high pressure hydrogen is obtained. This is due to the fact that hydrogen moves from the adsorbed phase, which is denser, to the bulk gas phase in a confined tank volume when the temperature increases. Hence, the potentially achievable pressure level depends strictly on the final temperature, on the volume available for the bulk gas phase inside the tank and on the mass of adsorbent (51).

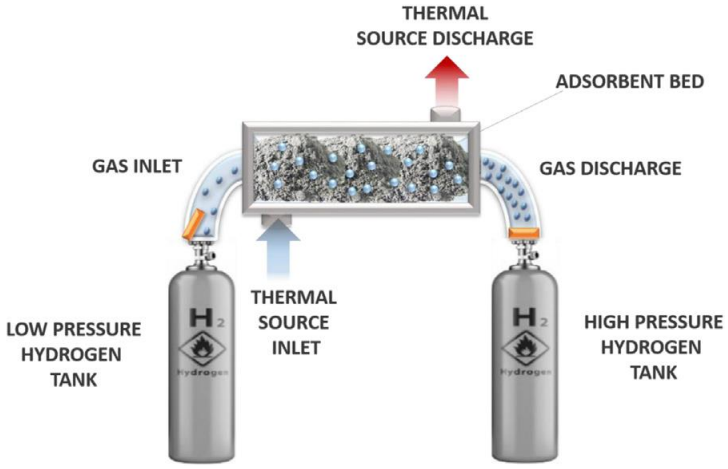

Figure 8: An adsorption compressor

An in-depth comparison between hydrogen cryogenic compression and adsorption compression was carried out (39). It was found that both technologies have their advantages and indeed that it is difficult to select one as the best solution. On the one hand, adsorption compression offers the advantage of lowering the pressure needed to store a given amount of hydrogen which is an important advantage in terms of safety. In addition, they do not have any moving parts and operations are vibration free which both crucial requirements for long-term operation are. On the other hand, the additional mass due to the presence of adsorbent material can be detrimental for applications in which weight is crucial, e.g. for the aerospace sector. Moreover, the adsorption compressor is affected by thermal management issues. Finally, hydrogen storage by adsorption at low pressure offers more advantages than mechanical compressed gas, such as: (i) lower costs and (ii) a higher amount of hydrogen stored compared to simple compression in an empty vessel, for low pressures applications and in room temperature conditions, using specific activated carbons (52).

2.2.4. Metal hydride compressors

Metal hydride compressors ensure efficient hydrogen compression without any moving parts such as solid or liquid pistons or diaphragms. They are also commonly known as “thermally driven” compressors because they use the properties of hydride-forming metals, alloys or intermetallic compounds to adsorb and desorb hydrogen simply by means of heat and mass transfer in the reaction system. A metal hydride hydrogen compressor essentially consists of a stainless steel tank containing the metal hydride and a heat source/sink as presented in Figure 9 below.

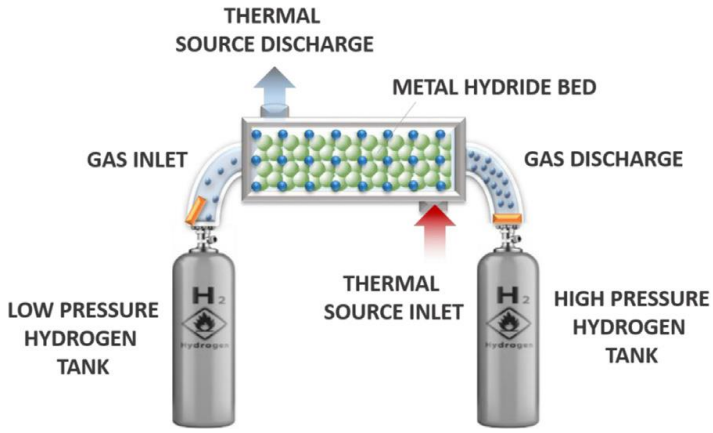

Figure 9: A metal hydride compressor

When low-pressure hydrogen is introduced into the metal hydride tank through the central artery, it spreads in the metal hydride bed and hydrogen exothermic adsorption occurs. Adsorption starts at low temperature and continues until the equilibrium pressure is equal to the supply pressure. To evaluate the equilibrium pressure at which both metal-hydrogen solution and hydride phase coexist, Pressure-composition (P-c-T) isotherms specific to a given hydride-forming material are used. Once the equilibrium pressure is reached, hydrogen desorption can be carried out by supplying heat to decompose the metal hydride. Desorption produces an increase in the hydrogen pressure to the desired discharge pressure and allows a new P-c equilibrium to be reached. In brief, hydrogen compression is the result of the sequential cooling and heating of the metal hydride structure at it is controlled almost entirely by heat transfer (53). Natural air convection or forced air is generally used to manage heat transfer inside the reactor but an extensive number of applications are also based on water- or oil-cooling systems (54).
In this way, It is possible to carry out thermally-driven compression with a very simple design and operation, without moving parts and without problems related to wear, noise or intensity of energy used. Moreover, it is not necessary to use large volumes so the system is more compact and easier to integrate into infrastructures and hydrogen plants (55). With a high-temperature heat source, the achievable discharge pressure can be 3–10 times the supplied pressure with volumetric efficiencies of up to 93% (56). According to this, the real advantage of metal hydride compressors is that the system can be powered using waste industrial heat instead of electricity or a renewable energy source, particularly solar energy. These features can significantly decrease the system operating costs compared to those of mechanical compressors because electricity is certainly more expensive. High-pressure hydrogen can be obtained in situ from water by connecting metal hydride compressors to the outlet of an electrolyser thus recovering the electrolyser heat losses (57). Hydrogen refueling stations represent another interesting application for metal hydride hydrogen compressors, strengthened by the rapid development of fuel cell vehicles in

recent years. The latter application is feasible due to their high volumetric storage capacity, environment-friendliness and greater compactness than other typologies of compressors.

In order to achieve nowadays requirements of hydrogen compression of up to 70 MPa, multistage metal hydride compressor schemes are mandatory. In this, a series of coupled modules containing metal alloys with different equilibrium hydrogen pressures at the same temperature promotes the cyclical adsorption and desorption of hydrogen under specific thermodynamic conditions thus enabling a progressive increase of the outlet pressure. The development of such compressors requires a trade-off between the pressure level and overall efficiency to be achieved (58). The selection of well-suited hydride alloys is fundamental in order to obtain efficient hydrogen compression. Several requirements have to be satisfied, like high disassociation pressures at moderate temperatures, high hydrogen storage capacity, fast kinetics, easy activation (i.e., treatments to optimize sorption capacities and kinetics to obtain good charge-discharge cyclability) and low costs (59).

3. Simulation studies on MH and MH compression systems

In the 1980's, a number of mathematical models including one-dimensional conductive bed and two dimensional models were presented for metal-hydrogen storage systems (60). Although these were basic and included many simplifications in order to be solved by the available tools, they were the basis for future studies. Later, gas movement (mass convection) in heat transport throughout the bed was included in the energy balance calculations by Choi and Mills presenting a convective model taking into consideration gas movement and determining the gas velocity by Darcy's law (61).

Jemni and Nasrallah conducted a number of theoretical and experimental works on MH systems in the 1990's (62). They performed two-dimensional mathematical models and solved them to investigate the impact of parameters such as initial pressure and temperature and also the geometrical features of the vessel such as height to radius (h/R) on both adsorption and desorption processes. The bulk of their work has been devoted to evaluation of the preliminary assumptions applied in previous works. The shape of the reactor used was a small vertical cylinder with external cooling. The modified van 't Hoff equation for the equilibrium pressure fitted to experimental results with an order-five polynomial was used in their calculations.
They also presented modified expressions for reaction kinetics and examined them experimentally in a reactor containing a small amount of LaNi5 (2.6 g). Based on their results there was good agreement with the theoretical and experimental data in absorption while some differences could be observed in the desorption case, attributed to uncertainty in the pressure gauge. Another equation for equilibrium pressure with a ninth order polynomial was employed and evaluated with experimental and theoretical results that showed good agreement (63).

Following this, Askri et al. used the same reactor size and shape to study other parameters such as $(H/M)_0$ and the ratio of tank length to radius (h/R) in addition to taking into consideration the expansion volume in the calculations (64). Further, they presented a new method for the resolution of the governing equations in order to improve the computer implementation compared with previous methods (65). In these studies, assumptions such as expansion volume and pressure variation effect were evaluated and new kinetic equations and PCT isotherms were presented. Although Jemni and Nasrallah and Askri had performed extensive studies on the thermodynamics and kinetics of the MH systems, the geometrical features of the tank and the heat exchanger were still not the primary concern. Later, they concentrated on the heat exchange design for MH tanks. Four different shapes and configurations of cooling systems were examined to find the most efficient design. Based on their results, internal cooling using circular finned tubes in which a liquid fluid flows was the best option (66).

A study on the effects of geometrical features on the MH system performance was also performed by Mellouli et al. conducting a number of experimental and theoretical studies in which internal cooling with a spiral heat exchanger was used (67). Importantly, it was found that the heat exchange system with finned spiral tubes was superior to the spiral tubes without fins. They also found that the presence of transverse fins are necessary to improve heat transfer throughout the metal-hydride beds (68). It should be noted that gas velocity was not taken into account in these works. The analysis of coupled heat and mass transfer was performed disregarding the hydraulic issues.

Muthukumar et al. conducted several numerical studies on a horizontal hydrogen storage tank with a combination of internal concentric cooling tubes and external cooling jacket to investigate the effect of inlet pressure, cooling temperature and convective heat transfer coefficient on hydrogen storage

capacity, temperature distribution in the bed and the reaction rate (69) (70). They enhanced the heat exchanger by increasing the number of cooling tubes and investigated the impact of the configuration, dimensions and the number of the tubes on the hydriding performance, using the software packages Fluent and COMSOL to solve the governing equations, including Nishizaki's equilibrium pressure equation. The dimensions of the MH tank were higher than the previous studies (length 475 mm, internal radius 300 mm). However, the height to the radius (h/R) ratio was in the effective range which had been proposed by Askri.

Hardy and Anton constructed 2-D and 3-D models for a cylindrical hydrogen storage tank containing sodium alanate with a shell and tube type heat exchanger using COMSOL Multiphysics (71) (72). Although this model is comprehensive, some realistic features such as hysteresis and the volume expansion of MH during the absorption were not taken into account and the system geometries required optimisation.

Bhouri et al. used Hardy and Anton's results to investigate the effect of fin thickness, number and configuration of cooling tubes on the hydrogenation and dehydrogenation time on that system (73). Their intention was to maximize charging and discharging rates and minimize volume and weight fraction of the cooling system to the bed in order to achieve better system gravimetric and volumetric capacity. They also revealed the importance of the role of fins for metal-hydrogen tanks by determination of hydrogen sorption rates which were poorer in the absence of fins. Garrison et al. optimized the geometry of cooling systems with longitudinal and transverse fins based on maximizing gravimetric capacity of the hydrogen or minimizing the volume and dimensions of heat exchanger elements using the Nelder-Mead methods of builtin MATLAB routines. They concentrated on the hydrogen capacity based on the whole system weight including the heat exchanger.

Some researchers have used analytical methods for analysis and optimisation of the various parameters. Yang et al. defined analytical formula, mass controlled reaction rate and heat controlled reaction rate, to evaluate the system performance (74). They compared the obtained results with the numerical results which were found to be in agreement. Nyamsi et al. also presented an analytical model for a cylindrical MH tank containing LaNi5 to find the optimum fin dimensions using MATLAB built-in routines based on maximizing the effectiveness of the fins. Then they used the derived results in their numerical calculations with the COMSOL software package to see the effect of optimal fin design on the hydriding characteristics (75).

Raju et al. presented numerical studies on a sodium alanate system to optimise the geometrical parameters of both the container and exchanger using a COMSOL-MATLAB interface for three different designs, first a shell and tube type heat exchanger with sodium alanate in the tubes, secondly an internally helical heat exchanger and, thirdly, a shell and tube type heat exchanger with sodium alanate in the shell. Their modelling focused on the highest amount of hydrogen absorbed in a certain time (10.5 min which is 40% of refueling rate of the DOE 2010 goals) (76) (77).

Many efforts have been made to improve the basic MH mathematical models to obtain more realistic results. For this purpose, correlations were added to the numerical MH calculations or new parameters and definitions have been presented or reformulated. Minko et al. focused on finding accurate values of permeability (k), interphase heat transfer coefficient (H_{gs}), effective thermal conductivity (λ_e) and porosity (ε) for ordered and random packing of spherical MH particles by developing a direct numerical simulation (78) (79). Three different packing structures, simple cubic packing, body-centred cubic packing and face-centred cubic packing as well as random packing with sets of particle distributions and spheres of equal diameter with different porosity were considered in their work to determine corresponding values of H_{gs},

k and λ_e. These correlations and values were used in the mathematical model of the MH storage tank. Yang et al. proposed mass boundary conditions (flow coefficient) to determine hydrogen outlet flow and investigated the sensitivity to different parameters such as bed pressure, bed initial temperature and convective heat transfer coefficient. They also compared the effect of two types of internal heat exchange systems (electrical and convective heating) on the hydrogen outlet flow rate and found significant differences (80).

4. A 6-stage MHC

Operation principle of compression with metal hydrides

As mentioned in Section 2, a promising method for hydrogen compression, which does not consists of moving parts, is the compression with metal hydrides. This method uses a reversible heat-driven interaction of a hydride forming metal, alloy or intermetallic compound (M) with hydrogen gas to form a metal hydride (MH), which is further described in Eq (1).

$$M(s) + \frac{x}{2} H_2(g) \leftrightharpoons MH_x(s) + Q \quad (1)$$

The direct forward process of this reaction is called adsorption and results in the formation of MH accompanied with the release off heat (exothermic reaction), Q, equal to the absolute value of hydrogenation enthalpy $|\Delta H|$. The reverse process (desorption) results in endothermic hydride decomposition, requiring supply of approximately the same amount of heat at a higher operating temperature (81).

The equilibrium state of the reaction (1) is characterized by an interrelation between hydrogen pressure (P), concentration of hydrogen in the crystal lattice of the solid (C) and temperature (T). This relation is a unique characteristic feature of every hydride-forming material determining the thermodynamic behavior upon interaction with gaseous hydrogen and can be described through a PCT diagram.

At low concentrations ($0 \leq C \leq \alpha$), hydrogen atoms form an interstitial solid solution in the metal lattice (α-phase) with $C(H) \approx \sqrt{P(H_2)}$ according to Henry-Sieverts law. When the value of C exceeds concentration of the saturated solid solution (α), a precipitation of the hydride (β-phase) nucleates and the system ideally behaves according to the first-order phase transition law taking place at a constant hydrogen pressure, $P = P_P$ ($\alpha \leq C \leq \beta$). This pressure is referred as plateau pressure in the diagrams of metal-hydrogen systems. A further increase in hydrogen concentration is accompanied by the pressure increase corresponding to the formation of an H solid solution in the β-phase. When the concentration approaches a certain maximum value (C_{max}) corresponding to the maximum hydrogen capacity of the material, the equilibrium pressure exhibits an asymptotic increase, $P \rightarrow \infty$ (82).

The plateau width (β-α), is often considered as a reversible hydrogen capacity of the material, and the equilibrium of reaction (1) in the plateau region is described by the van't Hoff equation:

$$\ln\left(\frac{P_P}{P^0}\right) = -\frac{\Delta S^0}{R} + \frac{\Delta H^0}{RT} \quad (2)$$

where $P^0 = 1\ atm = 1.013\ bar$, ΔS^0 and ΔH^0 are standard entropy and enthalpy o hydride formation, and R is the universal gas constant.

Since the plateau pressure P_P increases exponentially with temperature, absorbing hydrogen in low-temperature and desorbing it in a higher temperature, will provoke a pressure increment of the outcoming hydrogen. This is the basic operation principle of a metal-hydride hydrogen compressor.

Development and set up of 6-stage MHC

The 6-stage MHC was set up and tested for compression of hydrogen from 7 bar, at which it is supplied, to a pressure more than 220 bar. The heating medium is water and it is planned to have a temperature of about 80 °C in order to simulate a solar thermal collector. The cooling takes place around 10 °C that can be supplied by running tap water. In a commercial application the cooling could be supplied by solar adsorption coolers. The heating and cooling medium that is used is water. The MHC consists of 6 metal hydride tanks that consecutively compress the hydrogen. The tanks in which the metal hydride material is stored are identical for each stage. The hydride forming material is different for each stage. Bellow, in Figure 10, a flow sheet of the MHC is shown.

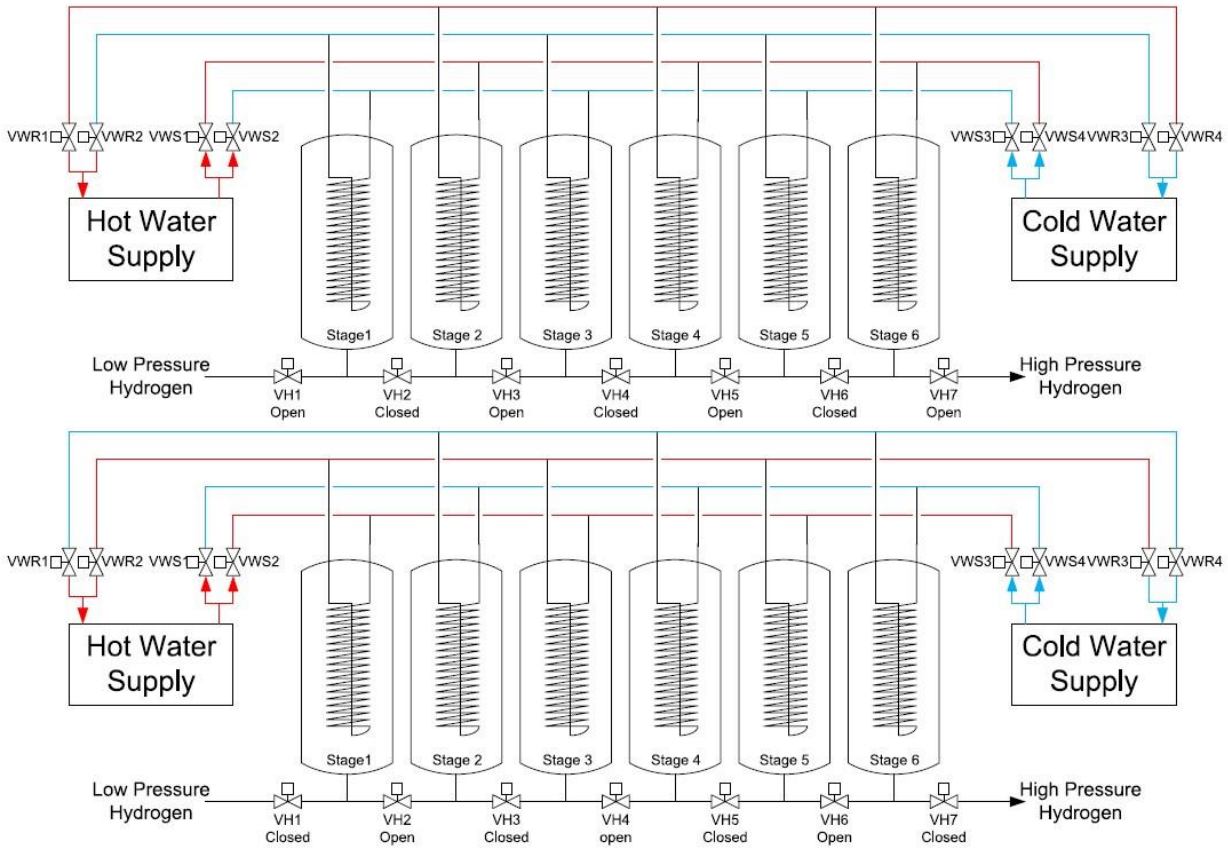

Figure 10: The flow sheet of Hystore's MHC

The flow sheet is shown in two different phases of operation. The top one shows the phase where the stages 1, 3 and 5 are cooled while the stages 2, 4 and 6 are heated (phase 1). In this phase, the Valves VWR1, VWS1, VWS3 and VWR3 are open on the water side, while the others are closed. On the hydrogen side, it is shown in the figure which valves are open and closed. Those stages that are cooled adsorb hydrogen in this phase, those that are heated desorb hydrogen. In the lower flow sheet, phase 2 of the operation is shown. In this Phase VWR2, VWS2, VWS4 and VWR4 are open on the water side and stages

1, 3 and 5 are heated while stages 2, 4 and 6 are cooled. It can be seen that the overall system only takes up and releases hydrogen in Phase 1, not in Phase 2.

Metal hydride stages

The metal hydride tanks of the MHC consist of a jacketed tube, where the metal hydride is located in the inner tube and the heating/cooling water runs through the annulus between the inner and outer tube. In addition to that, to improve the heat transport inside the packed bed of metal hydride, a copper tube coil, through which the water flows, is immersed in the packed bed. The front and rear parts of the jacketed tube are closed. On the front part a single connection is located for the hydrogen to enter and exit the inner tube. On the rear part, connections to and from the copper tube coil are implemented. The outer tube has connections radially located towards the front and the back for the water to enter and exit. One of those can be seen in figure 11. In figure 12, the back part of the inner tube with the inlet and outlet of the copper tube coil can be seen. The gap between the copper tube and the metal hydride container is later closed with fitting. In figure 13, the copper tube coil is shown. In figure 14, the front part of the inner tube is shown with the opening for hydrogen inlet and outlet. In figure 15 the readily assembled container can be seen, with the insulation applied to the most of the system. Finally, in figure 16 the complete and readily assembled MHC can be seen. On the left hand side of the figure the front view with the hydrogen piping and connections can be seen. On the right hand side of the figure, the back side with the piping to the coiled water tube and jacket can be seen.

Figure 11: Complete MHC container

Figure 12: Back part of inner tube

Figure 14: Copper coil tube

Figure 13 Front part of the inner tube

Figure 16: Assembled stage

Figure 15 The complete MHC

The results of the operation of the prototype MHC are summarized in Figure 17. Duriing the operation of the MHC, the pressure conditions of all stages was recorded indicating the coupling process of dehydrogenation and hydrogenation between stages.

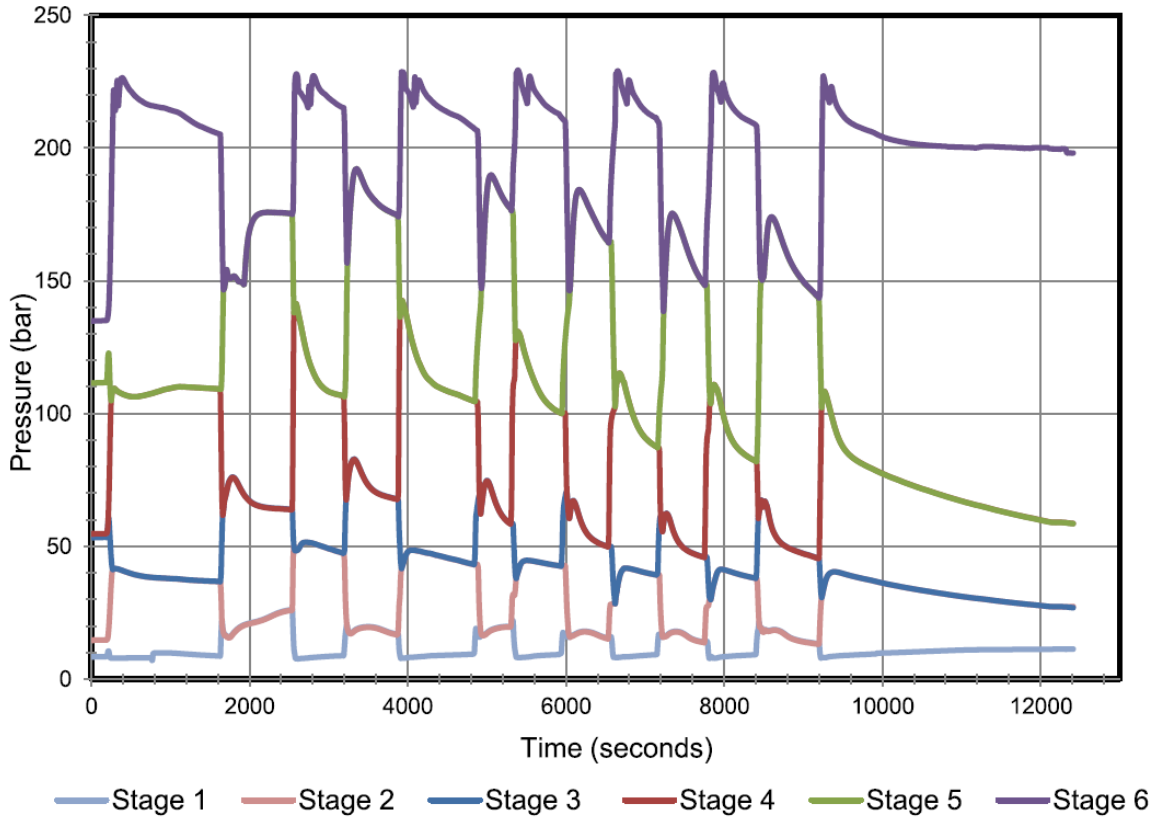

Figure 17: The pressure conditions during the operation of the MHC

Geometrical characteristics of metal hydride tanks components

As described above, the main components of each metal hydride tank are a copper coil and two stainless steel tubes, one that will be under pressure and the jacket forming one that is needed for heating and cooling. Bellow in Tables 1-3 the dimensional characteristics of each metal hydride tank component are presented.

Coil characteristics	Character	Units	Value
Tube Radius (minor)	Rt	mm	1.5
Tube thickness	ThC	mm	1.5
Tube Length	LC	mm	6
Tube volume	VC	m^3	42.4115 * 10-6
Coil Radius (major)	RC	mm	12.5
Coil Length		m	1.4
Cross section Area	AC	m^2	7.069 * 10 -6
Coil axial pitch	PC	mm	10.5

Table 1: Coil dimensions characteristics

Inner tube characteristics	Character	Units	Value
Radius	Rit	mm	21.425
Thickness	Tit	mm	8.74
Length	Lit	m	1.5

Table 2: Inner tube dimensions

Outer tube characteristics	Character	Units	Value
Radius	Rot	mm	37.15
Thickness	Tot	mm	1.5
Length	Lot	m	1.54

Table 3: Outer tube dimensions

The selection of the materials for MHC

First of all, the metal hydride materials are a crucial component in design of a metal hydride compressor, because the PCT curve has to face the demand of the compression process. Furthermore, in multi-stage compressors, different materials have to be found that can be well connected, i.e. the desorbing pressure of the first stage at the higher temperature has to match the adsorbing pressure of the second stage at the lower temperature. Also, the desorbing pressure of the second stage at the higher temperature has to match the adsorbing pressure of the third stage at the lower temperature and so forth. Therefore, in the past, some effort has been put into material characterization and it is still ongoing. A list of the most critical requirements that the MH material should fulfill are described below:

- PCT characteristics allow a compression from the lower pressure to the required higher pressure at the available temperatures TL and TH.
- The reversible storage capacity of the material should be high in order to eliminate the material that is needed for a given compression capacity.
- Fast kinetics so as to reduce the required material for a given compression capacity.
- Low slope of plateau pressure in order to achieve high compression ratio.
- Low hysteresis so high compression ratio can be achieved.
- Cycle stability.
- Tolerance on impurities.
- Availability of required scales at affordable costs.

The multitude of available materials for storing hydrogen can be divided into those that only bind the hydrogen by physisorption, which is a weak bond with low heat of reaction (<10 kJ/mol) and those that bind the hydrogen in chemisorption (and bulk adsorption), which is a strong bond with high heat of reaction (>10 kJ/mol). For application in metal hydride compressors, only materials of the second type are usually considered. Among these, two well-known material types are AB2 and AB5 type alloys.

Development's requirements of the 6-stage MHC, suitable materials for hydrogen compression was chosen. The MH type and the composition of the selected materials that were used in the MHC are presented bellow on Table 4.

MH code name	MH Composition	MH type
LN603-2	La Ce Ni	AB_5
T9	Ti Zr Cr Mn Fe V	AB_2
T3	Ti Zr Cr Mn Co	AB_2
T11	Ti Zr Cr Fe V	AB_2
VF26	Ti Zr Cr Fe V	AB_2
VF28	Ti Zr Cr Fe V	AB_2

Table 4: Material code names, composition elements and type

As mentioned above, one of the most important characteristics of metal hydrides is the pressure–composition–temperature (PCT) isotherm, from which a lot of parameters can be directly derived, including the enthalpy *ΔH* and entropy *ΔS*. The PCT curves represent the phase equilibrium of metal, gas and hydride under isothermal conditions. In the PCT diagrams, the applied gas pressure of the container is shown, over the actual concentration of the stored hydrogen.

MH code name	ΔH (ads)	ΔS (ads)	ΔH (des)	ΔS (des)
	J/molH_2	J/molH_2	J/molH_2	J/molH_2
LN603-2	25242	105	28195	107
T9	21466	94.62	26133	107
T3	20354	101	24823	109
T11	19991	100	20252	101
VF26	18198	98	19456	102
VF28	16232	95	18795	102

Table 5: Material calculated Enthalpies and Entropies

Alloy 1: LN603-2

PCT graph	Concentration (NL H_2) @ 200 bar & 10 °C
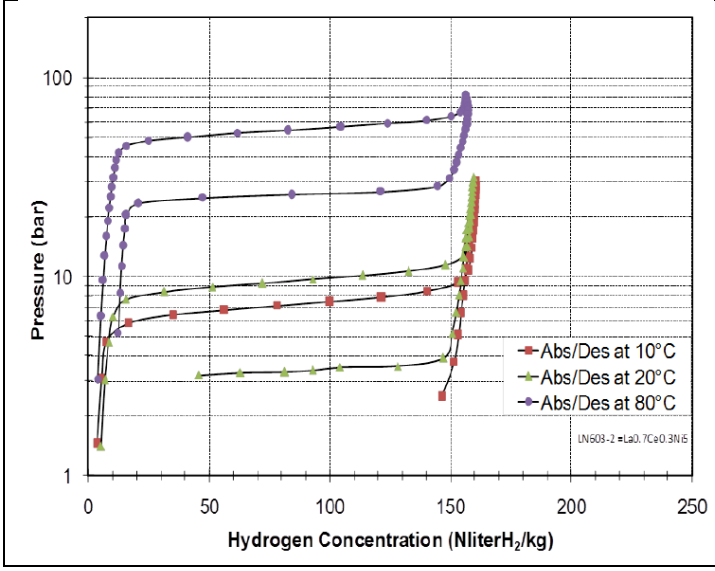	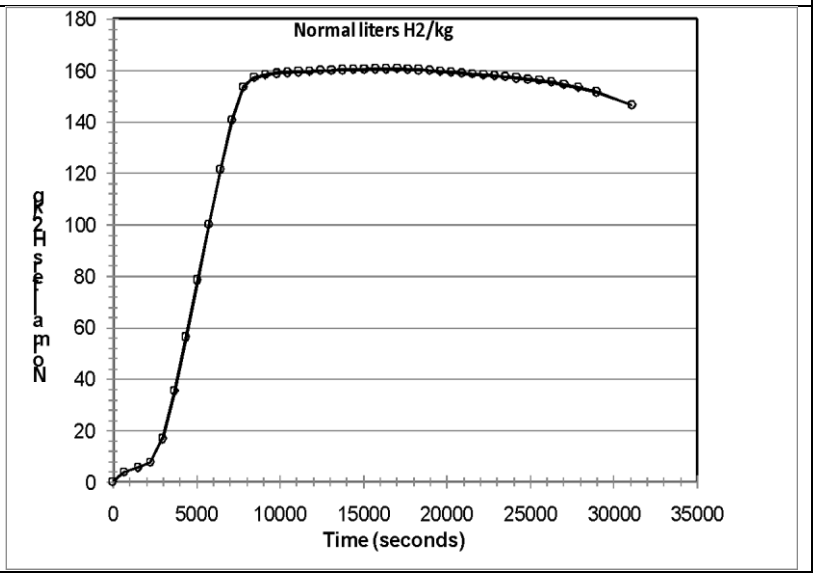

Table 6: Alloy 1 PCT and Concentration graphs

Alloy 2: T9	
PCT graph	**Concentration (NL H_2) @ 200 bar & 10 °C**
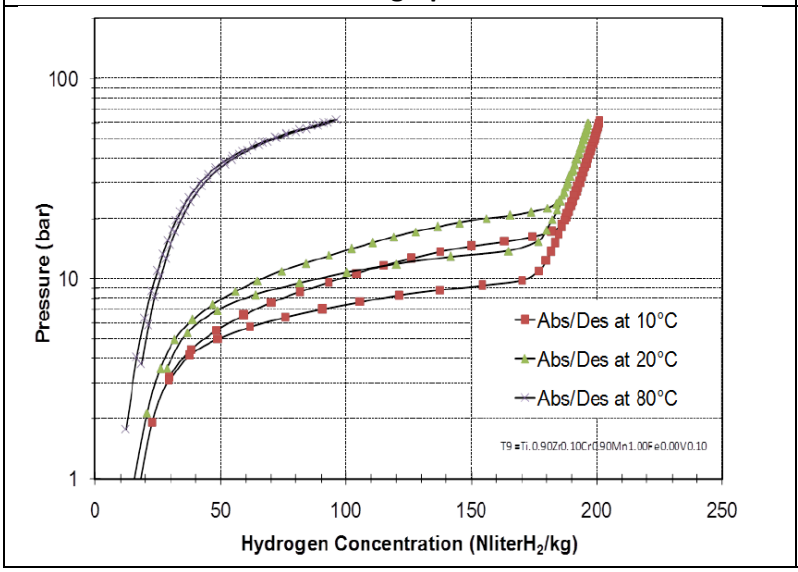	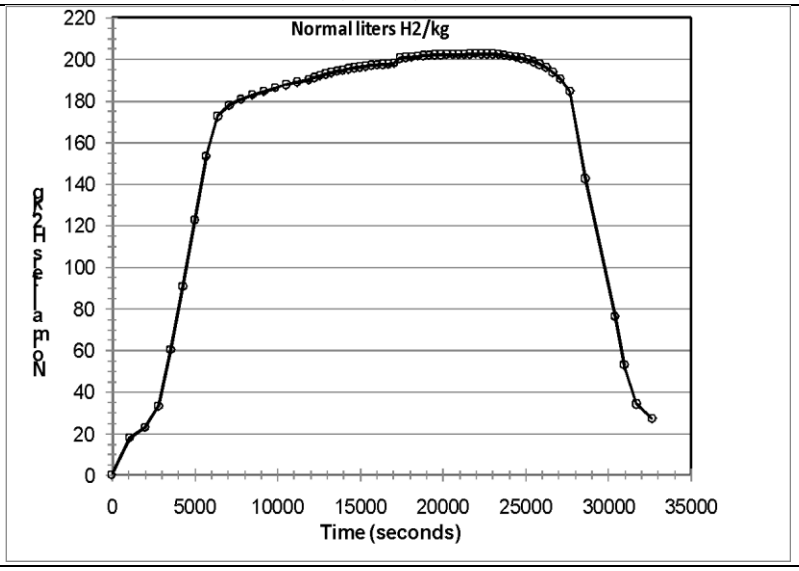

Table 7: Alloy 2 PCT and Concentration graphs

Alloy 3: T3	
PCT	**Concentration (NL H_2) @ 200 bar & 10 °C**
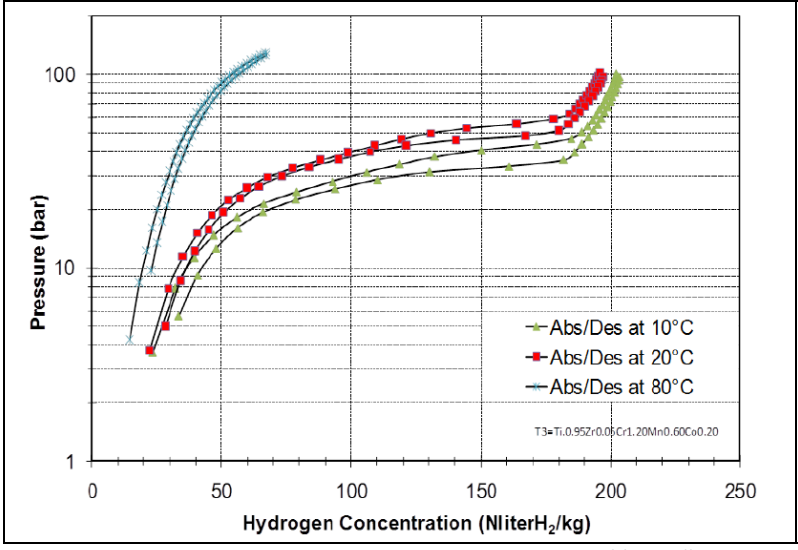	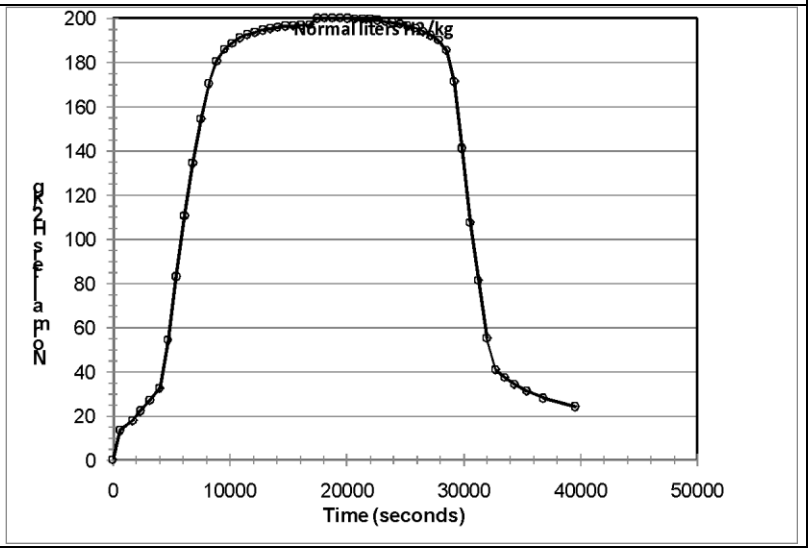

Table 8: Alloy 3 PCT and Concentration graphs

Alloy 4: T11	
PCT	**Concentration (NL H_2) @ 200 bar & 10 °C**
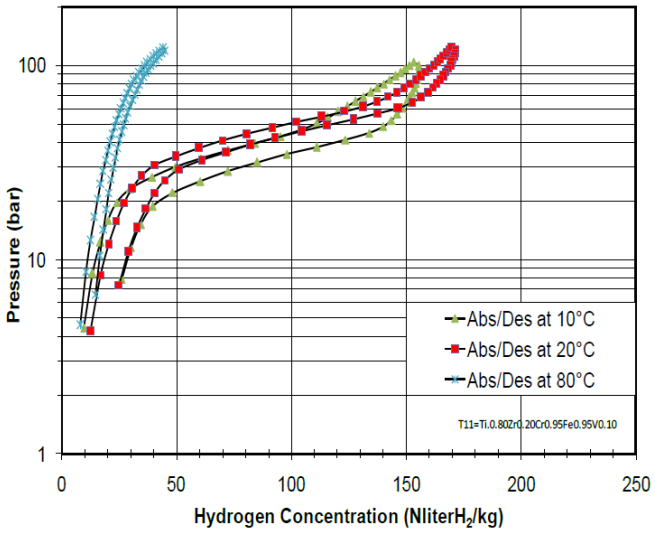	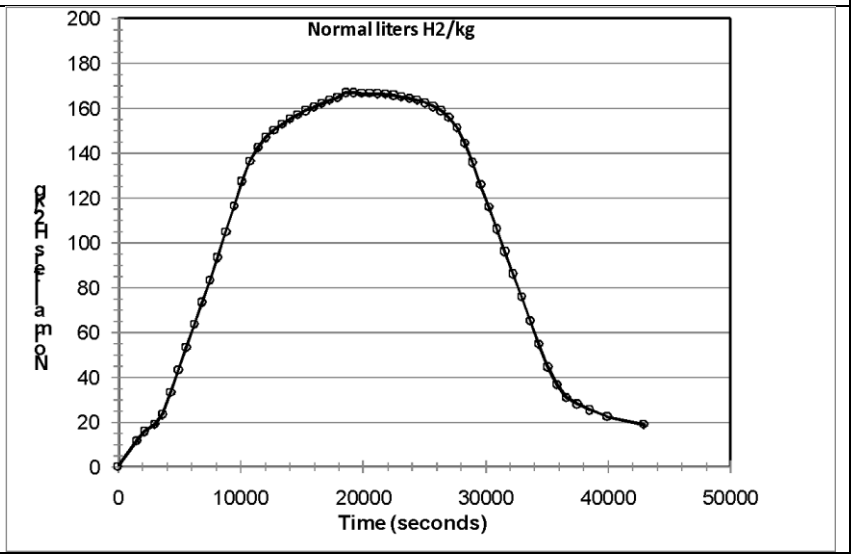

Table 9: Alloy 4 PCT and Concentration graphs

Alloy 5: VF26	
PCT	**Concentration (NL H_2) @ 200 bar & 10 °C**
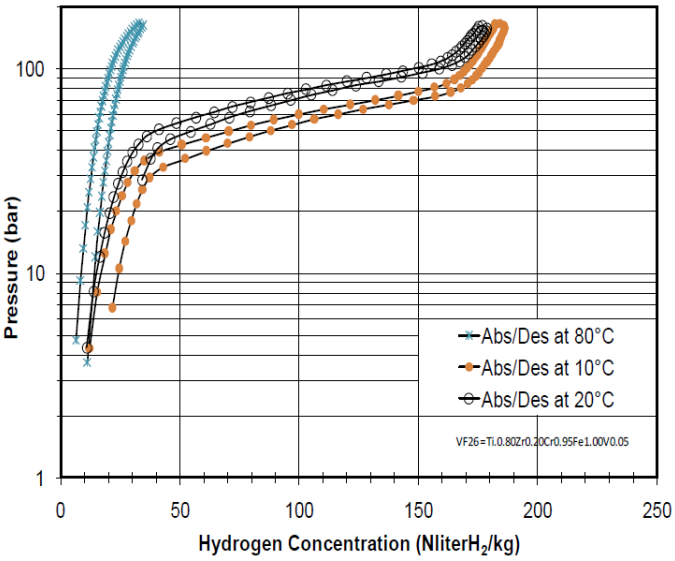	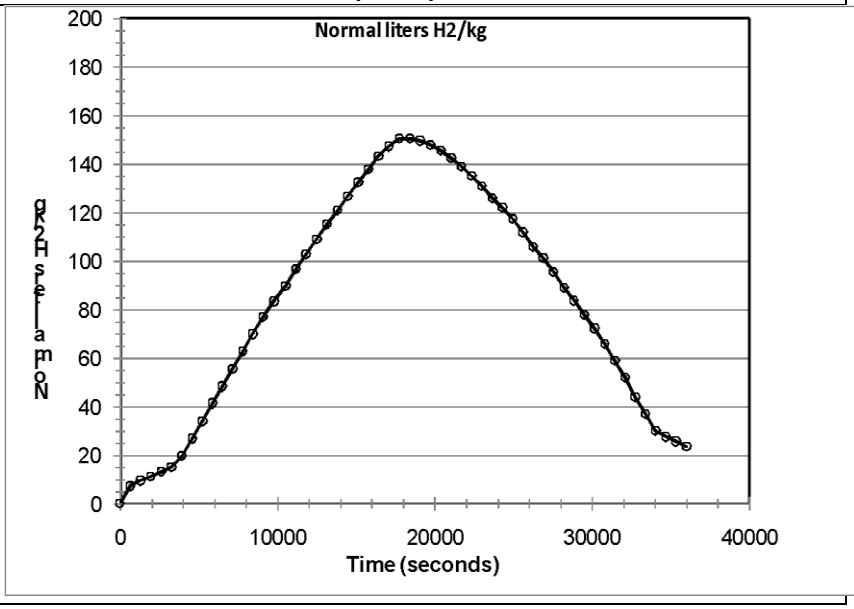

Table 10: Alloy 5 PCT and Concentration graphs

Alloy 6: VF28	
PCT	**Concentration (NL H_2) @ 200 bar & 10 °C**
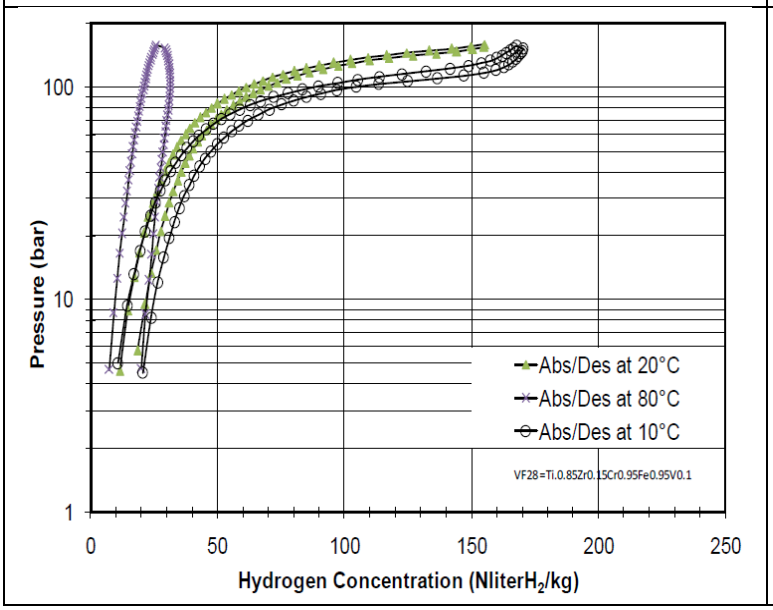	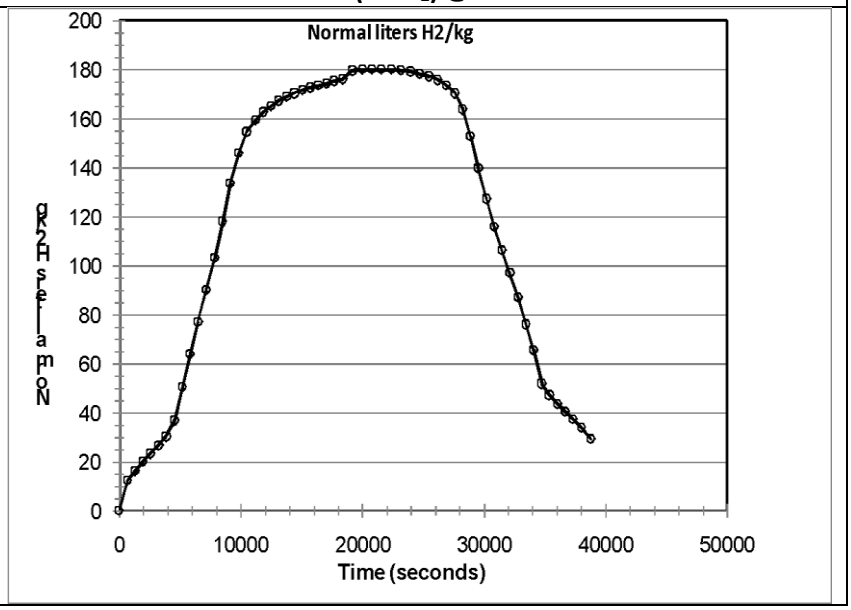

Table 11: Alloy 6 PCT and Concentration graphs

5. Numerical study on the 6-stage MHC

Modeling the behavior of a MHC

In general, a multistage hydride-based compressor consists of a series of coupled modules containing metal alloys, which store and release the hydrogen gas under certain conditions of temperature and pressure. The driving force, exerted by a variation in temperature, enables the transfer of hydrogen while it is increasing the exit pressure from one stage to another. For this reason, modeling the interaction procedure, between two successive stages, is required for the purpose of examining the total behavior and operating characteristics of a multistage-stage MH compression system.

A completed two-stage compression cycle comprises a hydrogenation process of first stage, a simultaneous dehydrogenation and hydrogenation process of first and second stage respectively, and a dehydrogenation process of the second stage in order to deliver the pressurized hydrogen. The same principal follows a multistage compression cycle, so modeling efforts were focused on simulating the simultaneous dehydrogenation and hydrogenation processes between every successive stage.

Theoretical approach – Numerical study of a two-stage MH compression system

For the needs of the numerical study, a two-stage coupling model was created, the dehydrogenation and hydrogenation processes of successive stages, are simulated in pairs (1-2, 2-3, 3-4, etc). The key factor during the coupling procedure is the appropriate matching of the plateau pressures of the successive stages. The plateau pressure for the dehydrogenation of every previous stage has to be higher than the plateau pressure of every next stage (P_1 @ T_H > P_2 @ T_L), so that the hydrogenating stage will be able to store hydrogen in a good rate.

Mathematical approach

Assumptions

For purposes of the current numerical approach, the following assumptions have been considered, simplifying the problem of hydrogen storage into the metal lattice:

a) Initially, the temperature and pressure profiles are uniform inside the MH bed.
b) Thermal conductivity and specific heat off the MH's are assumed to be constant during the compression cycle.
c) The MH and hydrogen gas are in local thermal equilibrium which implies that there is no heat transfer between solid and gas phases.
d) Radiative heat transfer and viscous dissipation are negligible.
e) Hydrogen can be treated as an ideal gas from a thermodynamic point of view.

Heat equation

Assuming thermal equilibrium between the hydride powder and hydrogen gas (Assumption c), a single heat equation is solved instead of two separate equations for both solid and gas phases:

$$(\rho \cdot Cp)_e \cdot \frac{\partial T}{\partial t} + \left(\rho_g \cdot Cp_g\right) \cdot \overline{v_g} \cdot \nabla T = \nabla \cdot (k_e \cdot \nabla T) + m \cdot \left(\frac{\Delta H}{M_{H_2}} - T \cdot \left(Cp_g - Cp_s\right)\right) \quad (3)$$

where $m\ (kg/s/m^3)$ represents the kinetic term.

The effective heat capacity is given by:

$$(\rho \cdot Cp)_e = \varepsilon \cdot \rho_g \cdot Cp_g + (1-\varepsilon) \cdot \rho_s \cdot Cp_s \quad (4)$$

for hydrogenation process, and

$$(\rho \cdot Cp)_e = \rho_g \cdot Cp_g + \rho_s \cdot Cp_s \quad (5)$$

for the dehydrogenation process.

The effective thermal conductivity is given by:

$$k_e = \varepsilon \cdot k_g + (1-\varepsilon) \cdot k_s \quad (6)$$

Hydrogen mass balance

The equation that describes the diffusion of hydrogen mass inside the metal lattice is:

$$\varepsilon \frac{\partial(\rho_g)}{\partial t} + div\left(\rho_g \overrightarrow{v_g}\right) = \pm m \quad (7)$$

where (-) is for the hydrogenation and (+) for the dehydrogenation process, and $\overrightarrow{v_g}$ is the velocity off gas during diffusion within the metal lattice (see eq. 9). From the assumption that hydrogen is treated as an ideal gas (Assumption e), hydrogen density is considered from ideal gas law:

$$\rho_g = \frac{P \cdot M_g}{R \cdot T} \quad (8)$$

Momentum equation

The velocity of a gas passing through a porous medium can be expressed by Darcy's law. Darcy's law describes the flow of a fluid through a porous medium and by neglecting the gravitational effect, is a simple proportional relationship between the instantaneous flow rate through a porous medium with permeability K (m2) and the pressure drop over a given distance and is given by:

$$\overrightarrow{v_g} = -\frac{K}{\mu_g} \cdot grad\left(\vec{P}_g\right) \quad (9)$$

where $K\ (m^2)$ is the permeability of the solid and $\mu_g\ (m^2/s)$ is the dynamic viscosity of gas.

Kinetic expression

In equations (3) and (7), the m term represents the amount of hydrogen that is stored in and released from the materials.

For the hydrogenations process:

$$m_{ads} = C_{ads} \cdot exp\left[-\frac{E_{ads}}{R_g \cdot T}\right] \cdot ln\left[\frac{P_g}{P_{eq}}\right] \cdot (\rho_{ss} - \rho_s) \quad (11)$$

For the dehydrogenation process:

$$m_{des} = C_{des} \cdot exp\left[-\frac{E_{des}}{R_g \cdot T}\right] \cdot \left(\frac{P_{eq} - P_g}{P_{eq}}\right) \cdot \rho_s \quad (12)$$

where C_{ads} and C_{des} are pro-exponential constants for adsorption and desorption respectively, E_{ads} and E_{des} the adsorption and desorption activation energy, ρ_{ss} the saturation density for hydride and ρ_s the density of the hydride at any time.

Equilibrium pressure

For the calculation of equilibrium or plateau pressure P_{eq}, the following equation was used:

$$P_{eq} = exp\left[\frac{\Delta H}{RT} - \frac{\Delta S}{R}\right] P_0 \quad (13)$$

Coupling mass and energy balance

The conditions of the system during the coupling between the dehydrogenating and hydrogenating stage after opening the connection valve is an important parameter that needs to be considered when trying to describe the compression cycle. The number of moles inside the interconnector between the two reactors at any time is given by the following relation:

$$n_{t+dt} = n_t + n_{des} - n_{abs} \quad (14)$$

where n_t and n_{t+dt} are the number of hydrogen moles in the total space at any time t and $t + dt$ respectively. The number of moles released from dehydrogenation process is n_{des} and the number of moles stored in hydrogenation process in a small time dt is n_{abs}.

The pressure of hydrogen inside the interconnector at any time is:

$$P_t = \frac{n_{t+dt} \cdot R \cdot T_c}{V_1 + V_2} \quad (15)$$

where V_1 and V_2 are the volumes of dehydrogenating and hydrogenating stage tanks and T_c is the temperature of the hydrogen gas inside the interconnector. Considering the pressure of hydrogen in the interconnector as the driving force for both dehydrogenation and hydrogenation process, the kinetic equations (11), (12) take the following form:

$$m_{ads} = C_{ads} \cdot exp\left[-\frac{E_{ads}}{R_g \cdot T}\right] \cdot ln\left[\frac{P_t}{P_{eq}}\right] \cdot (\rho_{ss} - \rho_s) \quad (16)$$

$$m_{des} = C_{des} \cdot exp\left[-\frac{E_{des}}{R_g \cdot T}\right] \cdot \left(\frac{P_{eq} - P_t}{P_{eq}}\right) \cdot \rho_s \quad (17)$$

Problem analysis

Chemical reaction analysis

The initial and saturation concentration of the materials should be calculated, so as to calculate mass of hydrogen that is released and stored during dehydrogenation and hydrogenation reactions. The following analysis is performed in order to calculate the concentration of the adsorbing/desorbing capacity of each material for hydrogenation and dehydrogenation.

From PCT data that was presented in Section 4, the maximum concentration of H2 that every material can adsorb was calculated.

$$C_A : \text{NL } (H2)/ \text{ kg } (M)$$

$$n_{H2} = C_A/22,4 \text{ [L/mole]}$$

As a consequence, we can compute the weight percentage of H2 adsorbed for every material.

$$wt\%=n_{H2}\cdot Mr_{H2}$$

AB_5 materials can adsorb 155 NL of H_2 per kg of material equal to 6,92 mole of H_2 with mass of 13.95 g.

AB_2 materials can adsorb 184 NL of H_2 per kg of material with 8.21 mole of H_2 and 16.56 g mass respectively.

For the requirements of the calculations all AB_2 materials will adsorb the same wt%.

Stage calculations

For the necessity of calculating the total amount of hydrogen adsorbed in each stage, the values of total mass, molecular weight, bulk and apparent density for every material was used.

m_M Mr_M, ρ_{Mb} bulk density, ρ_{Ma} apparent density $=0.73\cdot \rho_{Mb}$

The volume of alloy inside each stage will be:

$$V_{Ma}= m_M/ \rho_{Ma}$$

From the bibliography and empirical estimations hydride forming AB_2 and AB_5 materials expands their volume around 25% on hydrogenation. Therefore the volume of fully hydrogenated material will be:

$$V_{MH}=1,25\cdot V_{Ma}$$

Given the wt% of the adsorbed H_2 from each alloy and the stored total mass of hydrogen, in each stage will be:

$$m_{H2}=m_M \cdot wt\%/(1-wt\%)$$

The mole of hydrogen stored are:

$$n_{H2}=m_{H2}/Mr_{H2}$$

So, the final concentration of hydrogen mole per unit volume of the hydrogenated alloy will be:

$$C_H=n_{H2}/V_{MH}$$

The initial number of moles of M are:

$$n_M=m_M/Mr_M$$

and after hydrogenation,

$$n_{MH}=m_{MH}/Mr_{MH}$$

Accordingly, the initial and final concentration of moles per unit volume of the alloy will be:

$$C_i=n_M/V_{Ma}$$

$$C_f=n_{MH}/V_{MH}$$

m_M [kg]	Mr_M [g/mol]	V_M [m3]	ρ_{Ma} [kg/m3]	wt%	C_i [mol/m3]	C_f [mol/m3]
1.9771	432.74	0.000353799	4695.3	1.4	12913.53	10427.09
1.6613	159.03	0.000353829	5588.11	1.656	29524.02	23712.62
1.6613	157.5	0.000353829	5588.11	1.656	29810.83	23940.08
1.6613	157.08	0.000353829	5588.11	1.656	29890.53	24003.28
1.6613	159.78	0.000353829	5588.11	1.656	29385.44	23602.69
1.6613	164.35	0.000353829	5588.11	1.656	28568.33	22954.27

Table 12 Molecular weight and initial and saturation concentration of materials

Numerical model setup

Comsol multyphysics

The simulation software that is used for this purpose, is Comsol multiphysics. Comsol is a cross-platform finite element analysis, solver and multiphysics simulation software. It allows conventional physics-based user interfaces and coupled systems of partial differential equations. Comsol, provides an integrated development environment and enhanced multiphysics capabilities for thermal, mechanical, fluid and chemical applications, which is ideal for the simulation needs of the compressor.

Model Definition

Overall, a complete two stage compression cycle consists of one non-coupled hydrogenation process (first stage) followed by sensible heating, one coupled dehydrogenation (first stage)-hydrogenation process (second stage), a sensible heating process (second stage) and lastly, a dehydrogenation process (second stage). This model simulates the coupled dehydrogenation and hydrogenation process between two successive stages, with the intention of studying the real time operated behavior of a multy-stage MH compression system. The initial temperature of the hydrogenating and dehydrogenating stage is 10 ^{o}C and 90 ^{o}C respectively. The metal hydride characteristics were calculated from the selected materials of the first and second stage of the 6-stage MH compression system.

Geometry

A 3D model (figure 18) was chosen for a better representation of the real 6-stage MHC and more detailed results for a better understanding of the simulating process. A cylindrical geometry represents every tank which was selected to be filled up to 95% of Inner cylinder volume, with regard to match a design parameter of these systems. The porous metal hydride bed was described as a bulk geometry with a certain porosity for the purpose of model simplicity. The length of each reactor is *L=0.4m,* for the reduction of the computational required resources, and represents more or less the one third of the real system length. The heat management is achieved by the intermediate cylindrical shell and the cooper helical-shaped heat exchanger, where the heating/cooling medium circulates. At the center of the tanks, a hydrogen channel and a connector tube is placed and allows hydrogen to pass from dehydrogenation to hydrogenation stage. All dimensions that were used in the geometry of the model are the same with the real 6-stage MHC and they are presented on Tables 1-3.

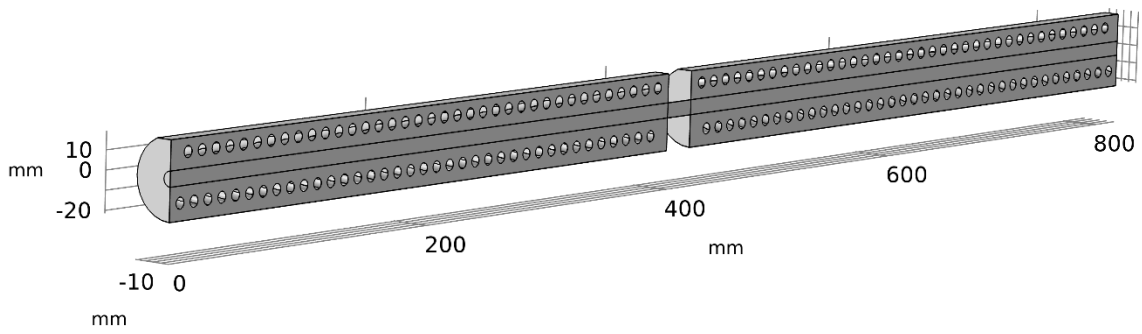

Figure 18: The geometry of the model

Physics setup

Three physical phenomena take place during the operation of a metal hydride compression system and they are heat transfer, mass transfer and chemical reaction phenomena. These phenomena are coupled and their interaction is dependent on time. The selected physics, which describe these phenomena on Comsol, are *Heat Transfer in Porous Media, Darcy's Law* and *Transport of Diluted Pieces*. Further description each of them is further analyzed bellow with the detailed set up of the numerical model. The indicated parameters and variables that are following, are described in detail on Tables 13-16.

Heat transfer modeling

Heat Transfer in Porous Media

Heat transfer phenomena occur in the whole geometry of the model. For the purpose of the simulation, the *Heat Transfer in Porous Media* module of Comsol was chosen because it describes better the modeling of heat transfer which takes place inside the porous metal hydride bed during the hydrogenation and dehydrogenation process (Figure 19).

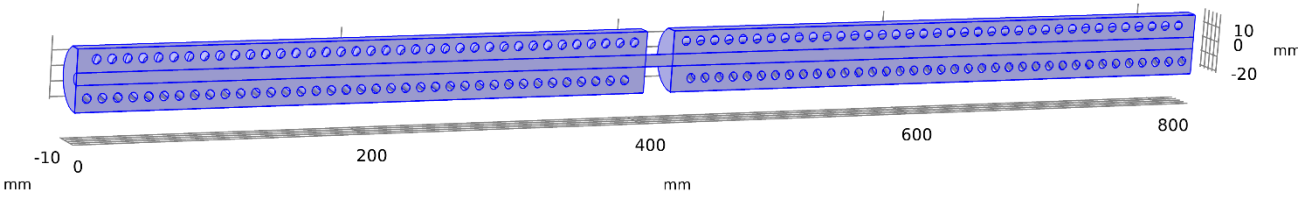

Figure 19: Heat transfer applied domains

Solving equations

$$(\rho C_p)_{\text{eff}}\frac{\partial T}{\partial t} + \rho C_p \mathbf{u}\cdot\nabla T + \nabla\cdot\mathbf{q} = Q + Q_{\text{vd}}$$

$$\mathbf{q} = -k_{\text{eff}}\nabla T$$

Boundary conditions

Desorption Stage - Heat sink

In order to describe heat suction from the reaction, a heat source boundary condition was chosen for the desorption stage (Figure 20). The heat generation equation is presented bellow and it consists of the reaction rate tau1, desorption fraction, volume fraction, density change during the reaction, entropy and enthalpy of formation

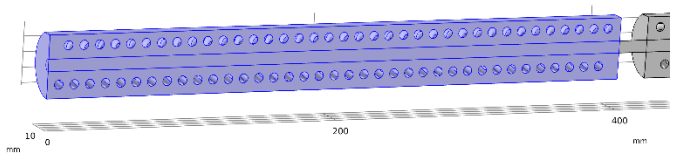

Figure 20: Desorption stage domains

and molar mass of hydrogen. The minus sign before the equation shows that this is a heat sink, which absorbs heat from the surrounded environment.

Q = -tau1*(des_fr)*(1-epsilon1)*deltar1*(deltaH_d/Mm_hy) [W/m^3]

Density change of the metal hydride during the reaction is described from the term deltar1 and it is updated from the concentration change of the reaction c on the *Transport of Diluted Species* module.

deltar1 = (c_sat1*Mm_mh1)-c*(Mm_mh1) [kg/m^3]

Adsorption Stage - Heat source

During adsorption process heat is generated. For this purpose, a heat source boundary condition was chosen for the adsorption stage (Figure 21). The heat generated equation is presented bellow and it contains the reaction rate tau1, the adsorption fraction, volume fraction, entropy and enthalpy of formation and molar mass of hydrogen. At this point, the 1-ads_fr term is the control mechanism of the heat source.

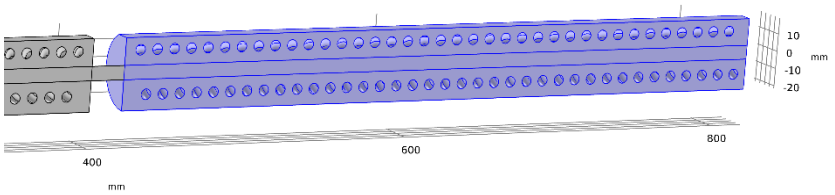

Figure 21: Heat source -Adsorption domain

Q = tau2*(1-ads_fr)*(1-epsilon2)*deltar2*(deltaH_a/Mm_hy) [W/m^3]

Density change of the adsorbing metal hydride during the reaction is described with the term deltar2 and it is updated from the concentration change of the reaction c on the *Transport of Diluted Species* module.

Deltar2 = (c*Mm_mh2-c_sat2*Mm_mh2) [kg/m^3]

Temperature

A temperature boundary condition was set both on the empty void where the coils pass and on the boundaries where the metal hydride beds touch the Inner tubes, as it is shown in Figure 22. For a better understanding of the other physics that take place in the numerical investigation, it is assumed that these domains are always in contact with a constant Temperature cooling and heating medium. The Temperature that values in these boundary conditions was set on 10 °C for the adsorption stage and 0 °C for the desorption stage.

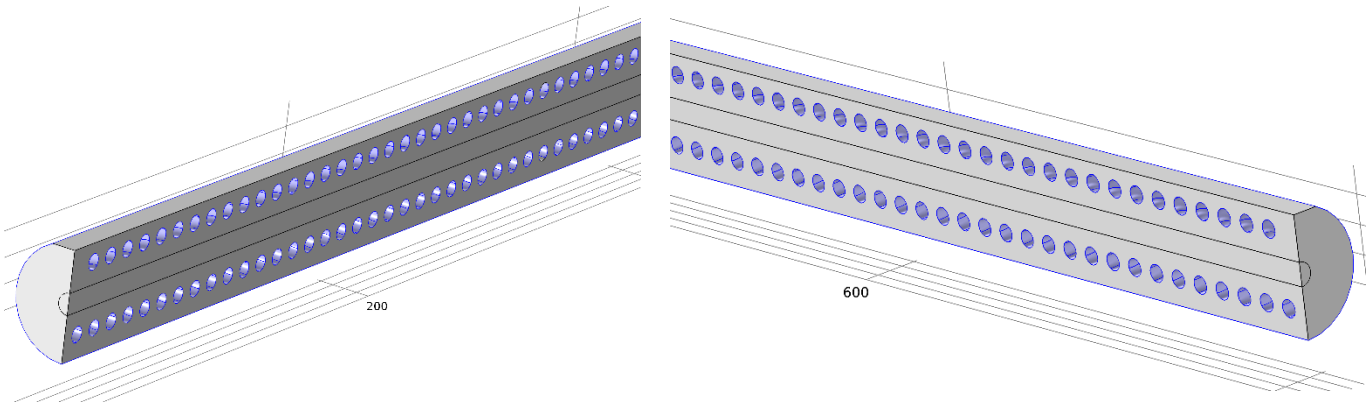

Figure 22: Temperature boundary conditions on coil and inner tube's touching areas

Thermal insulation

In the boundaries where no other boundary condition was set, a thermal insulation was automatically chosen by the program. Figure 23 illustrates the thermal insulated boundaries.

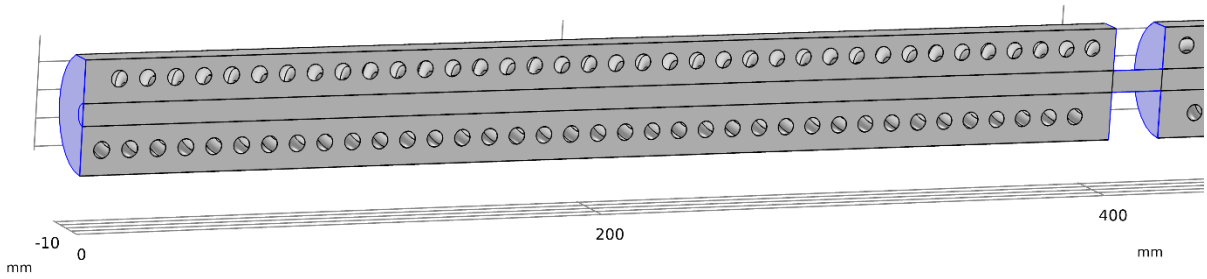

Figure 23: Thermal insulation boundaries

Porous media properties

Several heat transfer which is related to parameters of the metal hydride beds for both desorbing and adsorbing stages were set through the porous medium nodes. These parameters are presented below on Tables 13 and 14. Hydrogen which is related to parameters was automatically set through to be built in libraries of material properties on Comsol by adding the Hydrogen material on the fluid properties of porous media nodes. In addition to this step, velocity and pressure are being coupled with Darcy's velocity field and Absolute pressure computed through the *Darcy's Law* physics module.

Symmetry

A symmetry boundary condition was applied on the boundaries were the real geometry is cut in half, it is shown below in Figure 24.

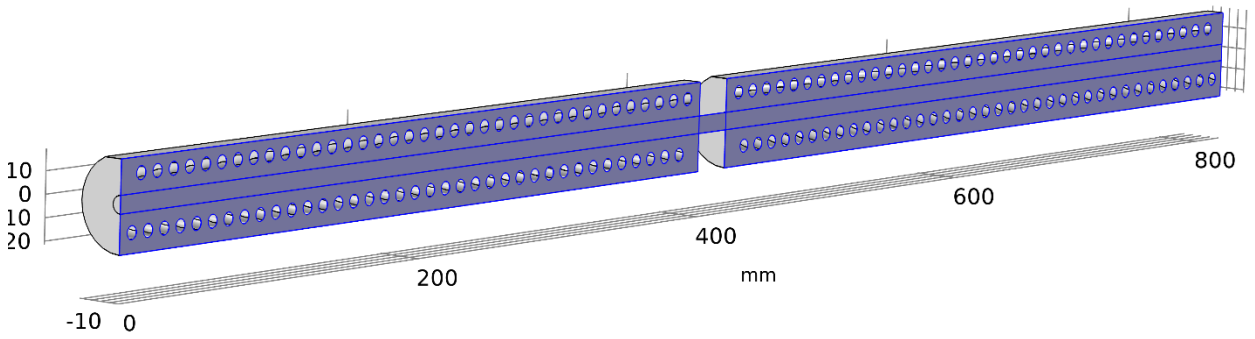

Figure 24 Symmetry boundaries

Initial values

The initial values on heat transfer domains, are temperature conditions. For desorption stage, the initial temperature was set at 90 °C and 10 °C for adsorption stage.

Chemical reactions modeling

For the needs of modeling the coupled chemical reactions of hydrogen desorption and adsorption of metal hydride beds, *Darcy's Law* and *Transport of Diluted Species* modules were chosen. Both of these features are required in order to model the pressure-controlled behavior of the adsorption and desorption reactions and the reaction rates of the phenomena.

Darcy's Law

The *Darcy's Law* module is used to emulate fluid flow through interstices in a porous medium. It is ideal for modeling low-velocity flows or media where the permeability and porosity are very small, and for which the pressure gradient is the major driving force, also the flow is mostly influenced by the frictional resistance within the pores. *Darcy's Law* module is applied on the whole geometry of the model as it is shown in Figure 25.

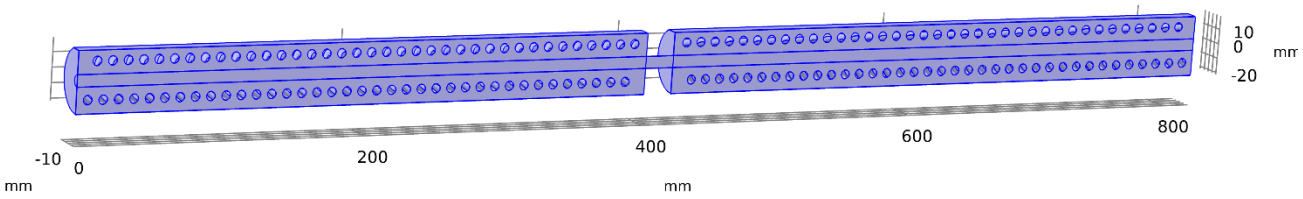

Figure 25: Darcy's Law domains

Solving equations

$$\frac{\partial}{\partial t}(\epsilon_p \rho) + \nabla \cdot (\rho \mathbf{u}) = Q_m$$

$$\mathbf{u} = -\frac{\kappa}{\mu}\nabla p$$

Boundary conditions

Desorption Stage – Mass source

A mass source boundary condition is applied on the domain of the desorption stage (Figure 20), for modeling the desorbed hydrogen from the metal hydride material. The mass source equation is conferred below and it contains the reaction rate tau1, the desorption fraction, the hydrogen density and the volume fraction. At this point, mass source is controlled through des_fr term which defines the dehydrogenation ratio of the material and it is affected by the concentration change c from *Transport of Diluted Species* module. A pressure condition is also added and it allows the mass addition when the pressure is below the plateau pressure of the material and it stops when pressure reaches plateau pressure or goes beyond its value.

Q_m = tau1*(des_fr)*rho_gas*(1-epsilon1)*(p<Peq1)+0*(p>Peq1) [kg/m^3*s]

Plateau pressure or equilibrium pressure is a unique characteristic for every material and it is related to the thermodynamic properties of the given material. The equation that refers to the plateau pressure is demonstrated below and the main parameters that characterize this quantity are Enthalpy and Entropy of desorption reaction at a given Temperature.

Peq1 = 1e5[Pa]*exp((deltaS_d/R_g)-((deltaH_d)/(R_g*T))) [Pa]

Adsorption Stage – Mass source

A mass source boundary condition is also applied on the domain of the adsorption stage (Figure 21), for modeling the hydrogen adsorption of the metal hydride material. The mass source equation is presented below and it consists of the reaction rate tau2, the hydrogen density and the volume fraction. Here mass source is controlled by 1 – ads_fr term which is driven from the concentration change c from *Transport of Diluted Species* module.

Q_m = - tau2*(1-ads_fr)*(1-epsilon2)*(rho_gas) [kg/m^3*s]

Plateau pressure or equilibrium pressure is a unique characteristic for every material and it is associated with the thermodynamic properties of the given material. The equation, that describes the plateau pressure, is shown below and the main parameters that characterize this quantity are Enthalpy and Entropy of desorption reaction at a given Temperature.

Peq1 = 1e5[Pa]*exp((deltaS_d/R_g)-((deltaH_d)/(R_g*T))) [Pa]

No flow

A no flow boundary condition was applied on the rest of the boundaries, where there is no movement of the hydrogen, which are indicated on Figure 26.

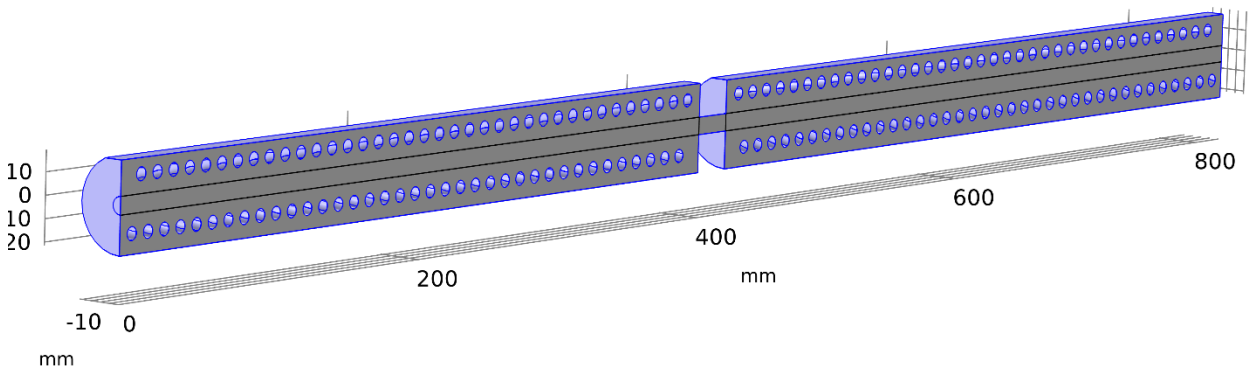

Figure 26: No flow condition boundaries

Symmetry

A symmetry boundary condition was applied on the boundaries, where the real geometry is cut as it is visible in Figure 27.

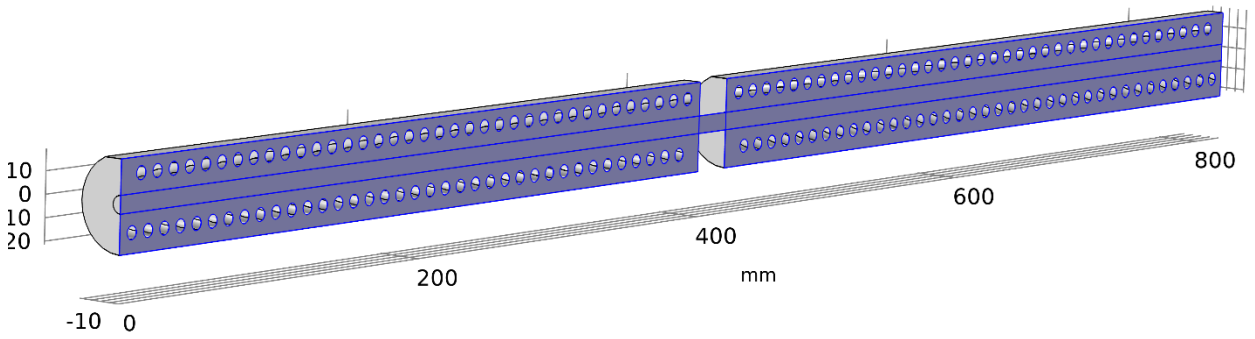

Figure 27: Symmetry boundary conditions

Fluid and matrix properties

The properties of the materials of the domains for the desorbing, the adsorbing stage and the connector were set through the Fluid and Matrix properties nodes, Figure 28. As things stand, permeability values were established on 1e-13 for the porous domains and 1e-6 for the connector domain. The porosity value for the connector domain was set at 1 in order to indicate that there is no porous medium there. The parameters of fluid properties were automatically set through built-in Comsol libraries for Hydrogen and for the metal hydride materials. The parameters are presented on Tables 13, 14. Moreover, the temperature was coupled with heat transfer temperature field computed through the *Heat Transfer in Porous Media* physics module.

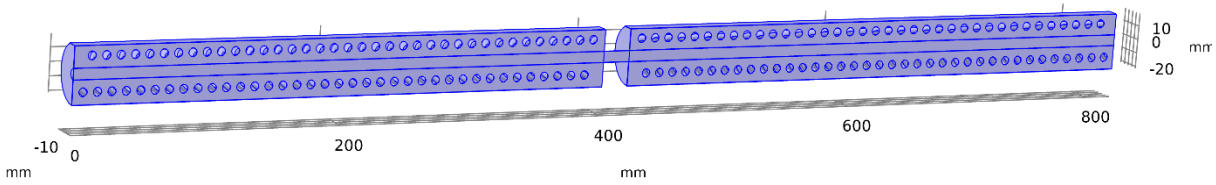

Figure 28: Porous and Matrix properties domains

Initial Values

The initial values of Darcy's law physics module were pressured conditions in all domains. For both dehydrogenating and hydrogenating, the initial values of pressure were set with the plateauf pressure of the materials at 90 ^{o}C (P_in1) and 10 ^{o}C (P_in2), respectively. For the hydrogen connector domain the term (P_in1*Va+P_in2*Vb)/(Va+Vb) was applied as the initial condition for the pressure in order to have the pressure average of the two stages.

Transport of Diluted Species

The *Transport of Diluted Species* module was used with the intention of calculating the concentration field of hydrogenation and dehydrogenation reactions, which can emulate transport and reactions of the species dissolved in a gas similar to a dilute solute in a solvent. For the transport mechanisms under the setting window, only Mass transfer in porous media was chosen, in order to enable porous media domains. Convection term is neglected due to minor velocity field that exists in these phenomena and the dependent variable, is the molar concentration, C. *Transport of Diluted Species* module is applied on the whole geometry of the model as it is shown in Figure 29.

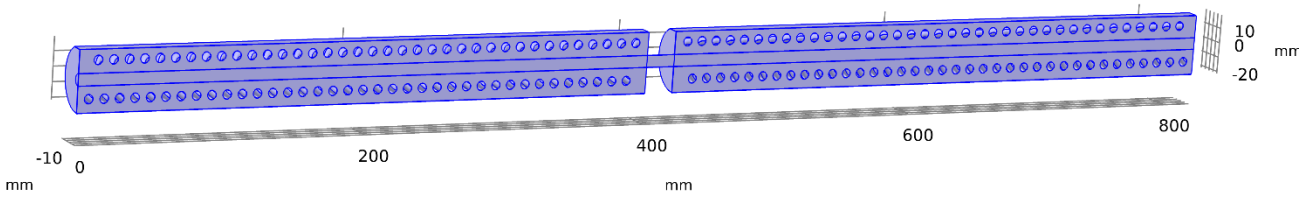

Figure 29: Transport of Diluted Species domains

Solving equations

$$\frac{\partial c_i}{\partial t} + \nabla \cdot \mathbf{J}_i = R_i$$

$$\mathbf{J}_i = -D_i \nabla c_i$$

Boundary conditions

Desorption Stage – Reaction

A Reaction boundary condition is applied on the domain of the desorption stage for modeling the dehydrogenation reaction that takes place in this domain. For this boundary condition the reaction rate equation was set and it consists of the reaction rate tau1 and the change of concentration of the metal hydride during this process, which happens only in the porous volume of this domain.

Rc = tau1*(c_sat1-c) [mol/(m^{3}s)]

The term tau1 represents the kinetic term of the reaction and it is described by the following equation where C_des is the kinetic constant, E_des the activation energy of dehydrogenation, Peq1 the plateau pressure of the metal hydride and p_t1 the pressure change of hydrogen gas in dehydrogenation stage. The term (Peq1-(p_t1))/Peq1) is the pressure controlled driving mechanism and T, which is computed from *Heat Transfer in Porous Media* module, is the temperature controlled mechanism. Coupling of mass balance will be further described below in this section.

tau1 = C_des*exp(-E_des/(R_g*T))*((Peq1-(p_t1))/Peq1) [1/s]

The term p_t1 describes the pressure increase in the total volume due to the increase of hydrogen moles in the free space from dehydrogenation process.

p_t1 = (n_t1*R_g*T)/(Va+Vb) [J/m^3]

Adsorption Stage – Reaction

A Reaction boundary condition is also applied on the domain of the adsorption stage in order to emulate the hydrogenation reaction that takes place in this domain. For this boundary condition the reaction rate equation was set and it contains the reaction rate tau2 and the concentration's change of the metal hydride with a minus sign that indicates the consumption of hydrogen mass, which occurs during this process. This boundary is only applied on the porous volume of this domain.

R_C = - tau2*(c-c_sat2) [mol/(m^3s)]

Similar to the dehydrogenation reaction, the tau2 term signifies the kinetic term of the reaction and it is described by the equation below, where C_ads is the kinetic constant of adsorption, E_ads the activation energy of hydrogenation, Peq2 the plateau pressure of the metal hydride and p_t2 the pressure change of the total volume due to hydrogen moles variation from hydrogenation reaction. Coupling of mass balance will be further described below in this section.

Tau2 = C_ads*exp(-E_ads/(R_g*T))*(ln((p_t2)/Peq2)) [1/s]

The term p_t2 explains the pressure increase in the total volume due to the decrease of hydrogen moles in the free space from hydrogenation process.

p_t2 = (n_t2*R_g*T)/(Va+Vb)

Coupling mass balance

As described in the mathematical modeling, the coupling of mass balance is achieved through determination of the moles' number that exist in each volume of the model, which is represented in equation (14). The moles of hydrogen that exist on the dehydrogenation stage, n_{des} , are described through n_t1 term, which is shown below, and they are coupled with pressure p from the *Darcy's Law* module and temperature T from *Heat Transfer in Porous Media* module. Similar to dehydrogenation stage, the moles that exist on the hydrogenation stage n_{ads} are calculated from the term n_t2. In this way, the coupling of mass balance is accomplished through pressure and temperature coupling.

n_t1 = (p*(Va))/(R_g*T)-(p*Vcon)/(R_g*T) [mol]

n_t2 = (p*(Vb))/(R_g*T)-(p*Vcon)/(R_g*T) [mol]

No flux

A no flux boundary condition was applied on the rest of the boundaries, where there is no transport of the hydrogen and they are indicatein Figure 30.

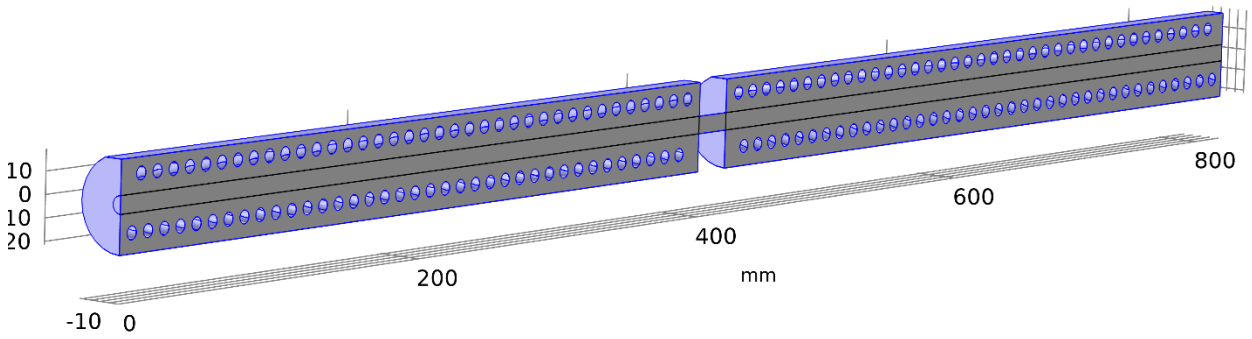

Figure 30 No flux boundaries

Symmetry

A symmetry boundary condition was applied on the boundaries were the real geometry is cut as it is pointed out in Figure 31.

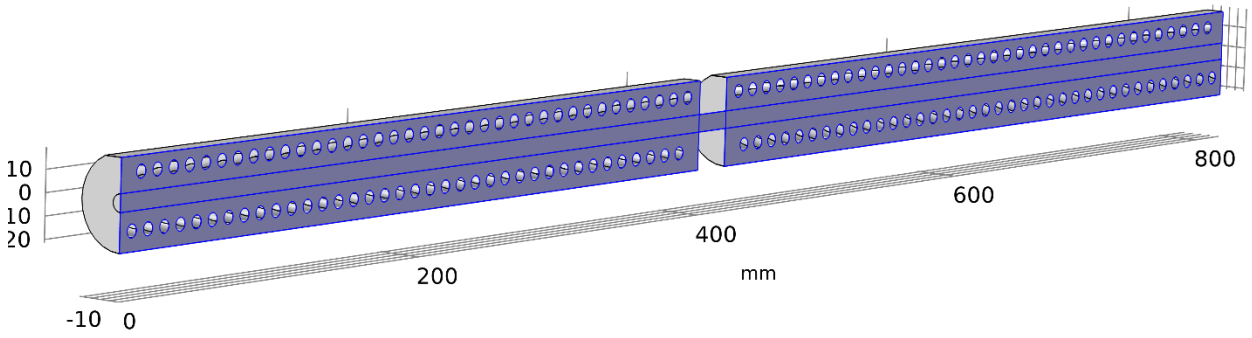

Figure 31: Symmetry boundaries

Transport properties

The transport properties of the materials of the desorption and the adsorption stage were set through the Transport properties nodes. The parameter which was defined here, is the Diffusion coefficient of the porous beds of the metal hydrides. The value of the properties was established at 1e-7 [m^2/s] for both cases of adsorption and desorption, according to the bibliography. In that case the temperature coupling T from *Heat Transfer in Porous Media* module was applied. The same approach was also applied on the connector domain.

Initial Values

The initial values for *Transport of Diluted Species* physics domains were the initial condition of concentration. For the chemical reaction analysis of that, was performed in previous section, the initial concentration values of each reaction was calculated and applied on this physic module. For the domain of the connector an initial minor value of 50 [mol/m^3], was set for the requirements of the computation.

Model parameters

Name	Expression	Value	Description
T_in1	90 [degC]	363.15 K	Initial temperature
P_in1	222.2[bar]	2.222E7 Pa	Initial pressure
c_in1	24003 [mol/m^3]	24003 mol/m³	Saturation concentration
c_sat1	29891 [mol/m^3]	29891 mol/m³	Initial concentration
deltaH_d	20252 [J/mol]	20252 J/mol	Enthalpy of formation
deltaS_d	101 [J/(mol*K)]	101 J/(mol·K)	Entropy of formation
C_des	55 [1/s]	55 1/s	Kinetic Constant desorption
E_des	25000[J/mol]	25000 J/mol	Activation Energy
Mm_mh1	157.08e-3[kg/mol]	0.15708 kg/mol	Molecular mass
Cp_mh1	280[J/(kg*K)]	280 J/(kg·K)	Specific heat
rho_mh1	5588.11[kg/m^3]	5588.1 kg/m³	Density
lambda_mh1	0.4 [W/(m*K)]	0.4 W/(m·K)	Thermal conductivity
epsilon1	0.7	0.7	Porosity

Table 13: Desorption parameters

Name	Expression	Value	Description
T_in2	10 [degC]	283.15 K	Initial temperature
P_in2	130[bar]	1.3E7 Pa	Initial pressure
c_in2	29386 [mol/m^3]	29386 mol/m³	Initial concentration
c_sat2	23602[mol/m^3]	23602 mol/m³	Saturation concentration
deltaH_a	18198[J/mol]	18198 J/mol	Enthalpy of formation
deltaS_a	98[J/(mol*K)]	98 J/(mol·K)	Entropy of formation
C_ads	55[1/s]	55 1/s	Kinetic Constant desorption
E_ads	25000[J/mol]	25000 J/mol	Activation Energy
Mm_mh2	159.78e-3[kg/mol]	0.15978 kg/mol	Molecular mass
Cp_mh2	280[J/(kg*K)]	280 J/(kg·K)	Specific heat
rho_mh2	5588.11[kg/m^3]	5588.1 kg/m³	Density
lambda_mh2	0.4 [W/(m*K)]	0.4 W/(m·K)	Thermal conductivity
epsilon2	0.7	0.7	Porosity

Table 14 Adsorption parameters

Name	Expression	Value	Description
Peq1	1e5[Pa]*exp((deltaS_d/R_g)-((deltaH_d)/(R_g*T)))	Pa	Equilibrium Pressure
tau1	C_des*exp(-E_des/(R_g*T))*((Peq1-(p_t1))/Peq1)	1/s	Desorption Kinetic
des_fr	(c_sat1-c)/(c_sat1-c_in1)*(c<c_sat1)+0*(c>c_sat1)	1	Dehydrogenation Fraction
rho_gas	(p*Mm_hy)/(R_g*T)	kg/m³	Density of h2
deltar1	(c_sat1*Mm_mh1)-c*(Mm_mh1)	kg/m³	
n_t1	(p*(Va))/(R_g*T)-(p*Vcon)/(R_g*T)	mol	
p_t1	(n_t1*R_g*T)/(Va+Vb)	J/m³	

Table 16: Desorption variables

Name	Expression	Value	Description
Peq2	1e5[Pa]*exp((deltaS_a/R_g)-(deltaH_a/(R_g*T)))	Pa	Equilibrium pressure
tau2	C_ads*exp(-E_ads/(R_g*T))*(log((p_t2)/Peq2))	1/s	Adsorption Kinetics
ads_fr	((c_in2-c)/(c_in2-c_sat2))	1	Hydrogenation Fraction
rho_gas2	(p*Mm_hy)/(R_g*T)	kg/m³	
deltar2	(c*Mm_mh2-c_sat2*Mm_mh2)	kg/m³	
n_t2	(p*(Vb))/(R_g*T)-(p*Vcon)/(R_g*T)	mol	
p_t2	(n_t2*R_g*T)/(Va+Vb)	J/m³	

Table 15 Adsorption variables

Mesh refinement study

For the needs of solving the model, an automatic Physics-controlled mesh generation of tetrahedral elements, was used. In order to examine the minimum element number that is required for an accurate solution, a mesh refinement study was performed. In this study, the model was re-solved on three progressively finer meshes and the results were compared. The meshes sizes that were tested as well as the total element number and degrees of freedom, are presented in the Table 17 below.

Mesh size	Number of Elements	Degrees of Freedom	Line type
Fine	21501	86904	Dot
Finer	138452	539605	Solid
Extra Fine	1256147	4763273	Dash/dot

Table 17: The examined mesh sizes

The results of the mesh refinement study are presented in Figures 1-3. The change of the solution was examined on the parameters of pressure, hydrogenation/dehydrogenation fraction and temperature. The results indicate a stabilization of the solution on the Finer and Extra Fine mesh sizes, where the solution is almost identical for all the investigated parameters. For this reason, the Finer mesh size, was considered as the optimal mesh size for the rest of the simulated coupling pairs.

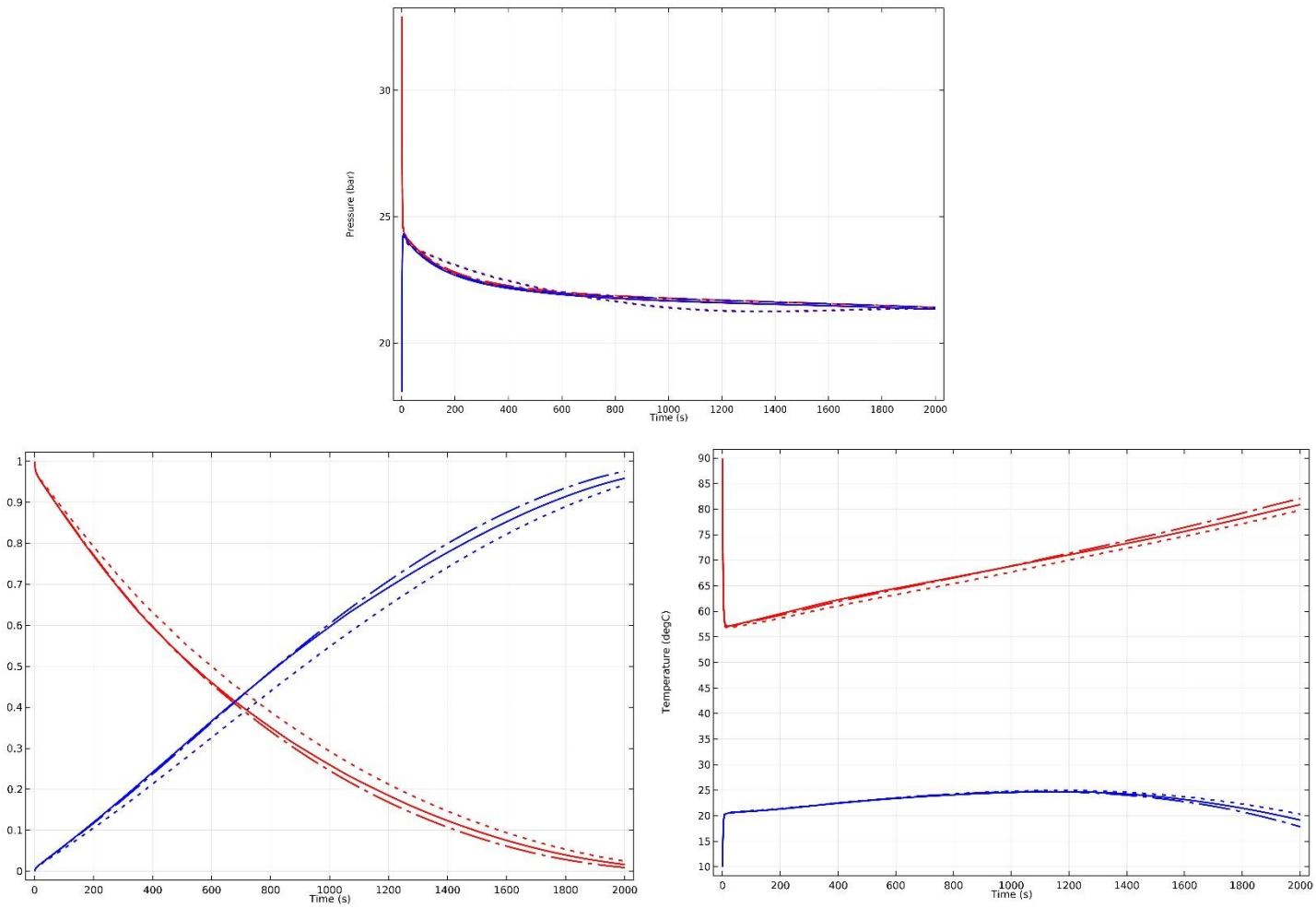

Figure 32: Dependence of the solution on three different mesh sizes

6. Results and discussion

The numerical modeling, of the coupled dehydrogenation and hydrogenation process, was achieved. The results that were obtained indicate the volume average of the dehydrogenating and the hydrogenating stage in all the examined parameters in order to benefit the uniform behavior of the system. With the purpose of confirming the correct physical behavior of this process, certain criteria must be fulfilled, which are described in detail below.

Hydrogenation/Dehydrogenation reactions

The most critical parameter is the completion of both dehydrogenation and hydrogenation reactions. This can be perfectly examined by the behavior of the hydrogenation and the dehydrogenation fraction respectively. Dehydrogenation fraction starts with a value of 1 and indicates that the material is fully saturated with hydrogen, and at the end of the dehydrogenation reaction, when all of the amount of the stored hydrogen is released, takes the value of 0. Respectively, hydrogenation fraction starts at the value of 0 and ends at 1, which indicates that the hydrogenating material has fully adsorbed the amount of hydrogen that was generated from the dehydrogenation process (Figure 33).

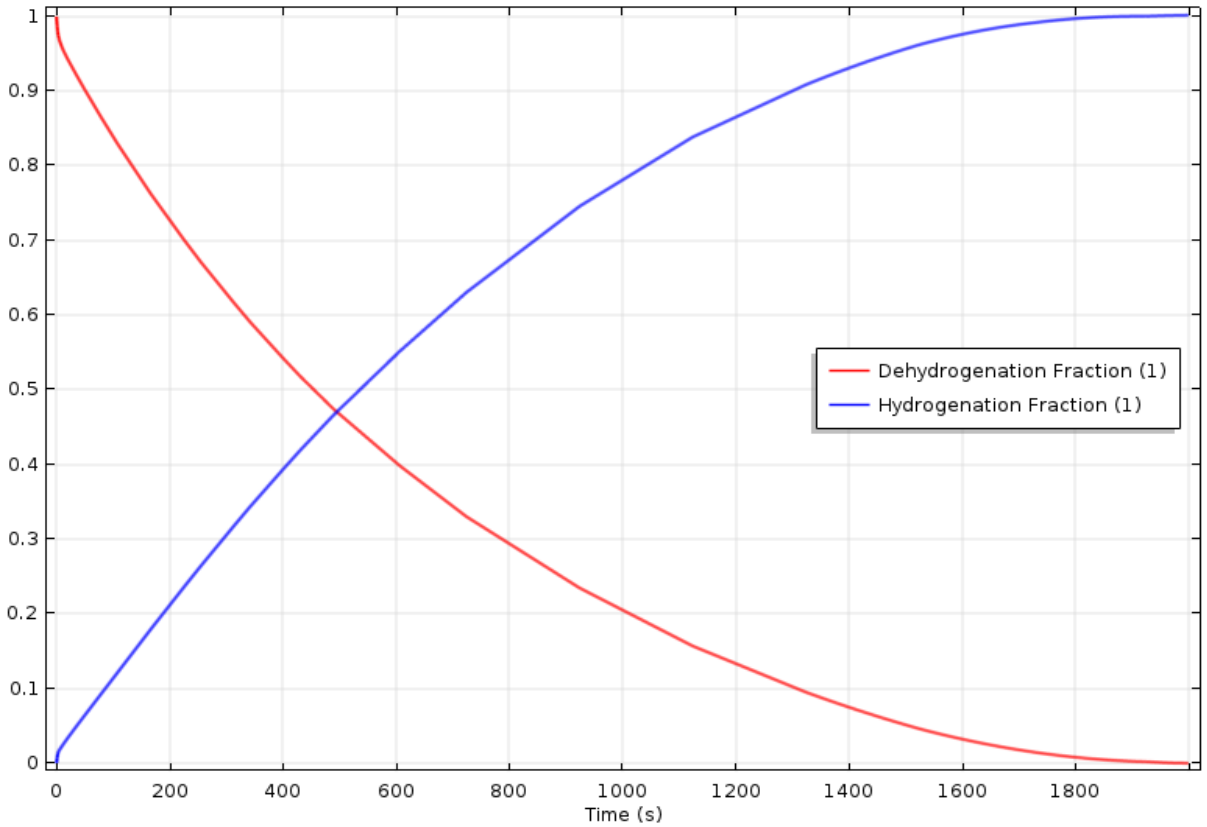

Figure 33: Results of hydrogenation and dehydrogenation fraction

A small delay in the time, which is about 80 seconds, is clearly evident in hydrogenation fraction that needs to reach the 50 % of its maximum value, in comparison to the dehydrogenation fraction. This happens because of the pressure difference of plateau pressure and actual pressure of each reacting material, which is bigger for the occasion of dehydrogenating stage, that indicates that these reactions occur faster than the hydrogenation reaction.

Pressure

Regarding pressure behavior, at the beginning of the process a rapid pressure balance should be achieved. Pressure should behave after this step regarding the behavior of the mass source and sink from the dehydrogenation and the hydrogenation stage. Furthermore, the temperature changes from heat generation and heat removal, from which is expected a change on the plateau pressures of the materials, but this is not as significant as the mass addition/ removal. From the real operation of the MHC (Figure 17) it is obvious that after the pressure balancing, there is an increasing effect on pressure and then there is a decreasing. This happens since the initial temperature on the starting point of coupling, the dehydrogenation stage has just stopped adsorbing so it was in a cool state (~10 °C) and the hydrogenating stage has just stopped desorption processes so it was hot (~ 90 °C). Until the adsorbing stage cool down to a certain temperature the plateau pressure of this material is high so it cannot start adsorbing immediately, or the kinetics are very slow. The reason why, this numerical investigation was not emulated in terms of the similar conditions, is that there is a sufficient variation on the values of enthalpy end entropy in those two temperature conditions and the results could not achieve a physical behavior.

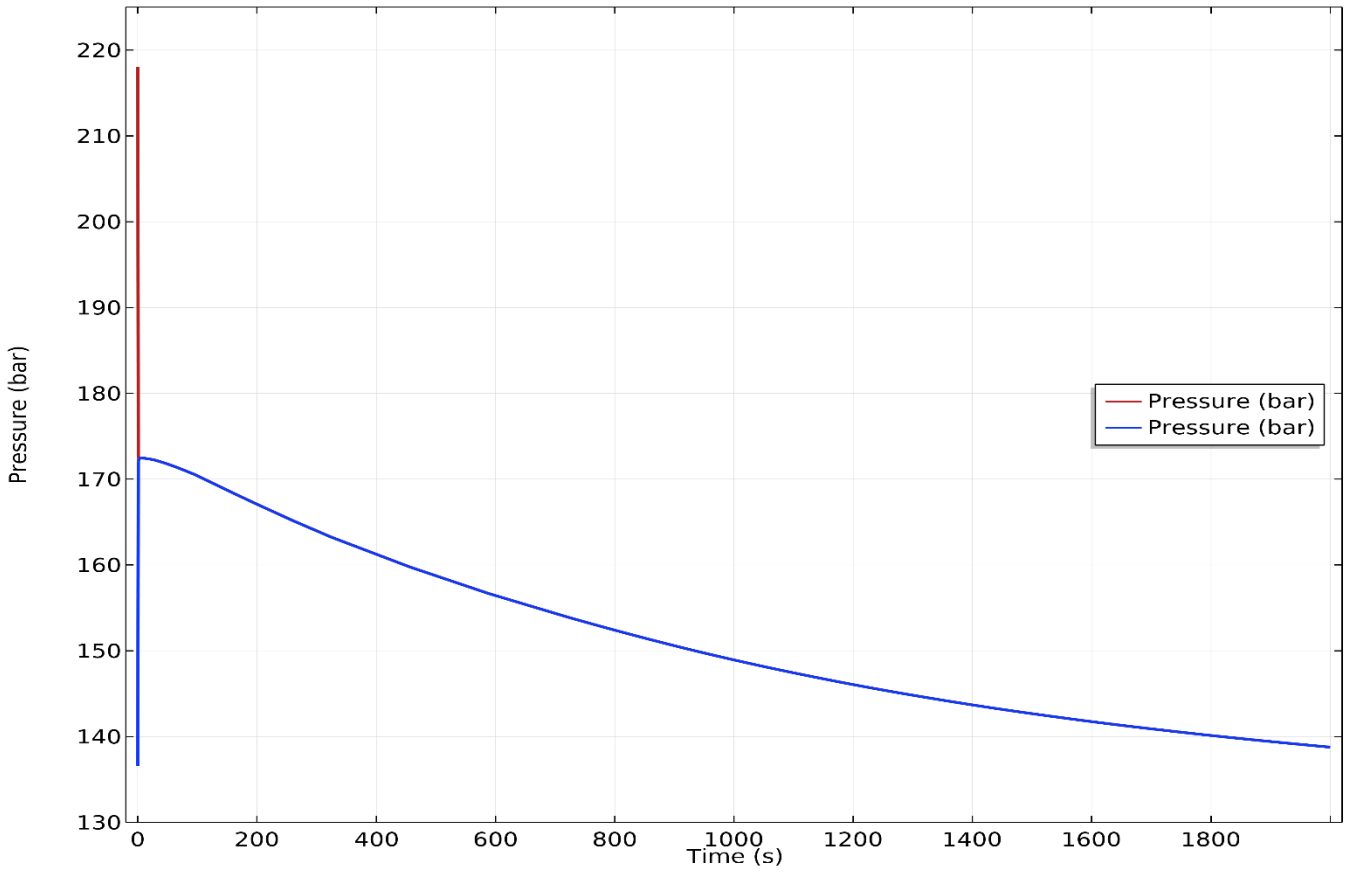

Figure 34 Results on pressure behavior

Pressure behavior also shows bigger values in comparison to the experimental data of the MHC (Figure 34). One reason is definitely, that the initial temperature conditions are opposite to the initial condition of the same process on the MHC. Another reason, is that there was not clear experimental data from the PCT curves for the high temperatures and there might be a mismatch on the values of enthalpy and entropy that was used to calculate the plateau pressure in those conditions.

Temperature

Temperature behavior is also another crucial result. The temperature of the dehydrogenating stage should rapidly drops because of the dramatic pressure decrease and the pressure balancing that occurs which enhances the dehydrogenation process. Also, the increase in the temperature should occur due to the hydrogenation process, as well. While time is passing the temperature of both stages should tend to their initial values due to the constant temperature boundary condition.

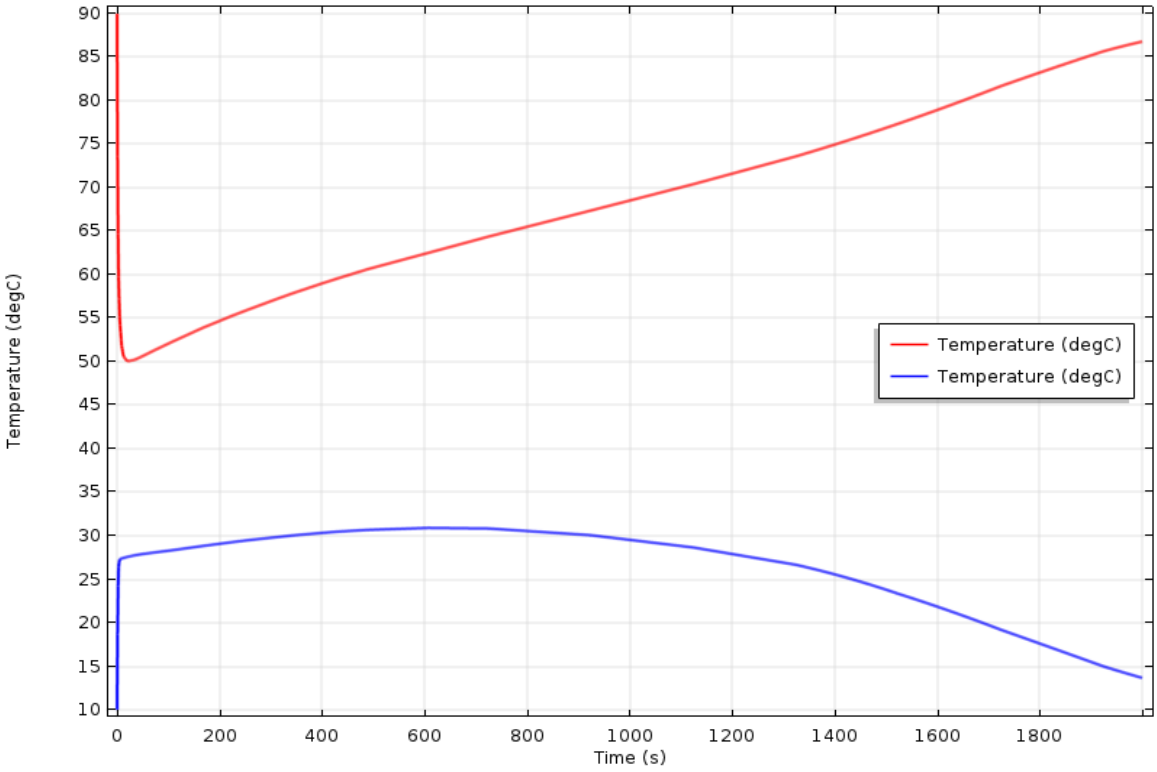

Figure 35: Results of Temperature behavior

The above described and expected behavior of temperature is stated in the results (Figure 35). A delay in the temperature increase of hydrogenating stage, is observed. This happens because of the delay of the hydrogenation process that is also obvious through hydrogenation fraction, in Figure 33.

The numerical study, of the coupled dehydrogenation – hydrogenation process of five, in total, successively pairs of stages (1-2 to 5-6), was performed. The simulation results that are listed below in Figures 36-40 and present the pressure, the dehydrogenation/hydrogenation fraction and the temperature's behavior of the emulated pairs.

In the following Table (18), the final pressure and the time period for hydrogenation and dehydrogenation are presented for each coupled pair. The hydrogenation and dehydrogenation time is estimated for percentages of fraction at 10%-90% and 90%-10%, respectively, so as to match the real working cycle of the compressor.

Coupling pair	Final Pressure	Dehydrogenation Initial Pressure	Hydrogenation Initial Pressure	Dehydrogenation time Fraction 90%-10%	Hydrogenation time Fraction 10%-90%
1st	21.17 bar	33 bar	18 bar	1369 s	1512 s
2nd	53.8 bar	76 bar	48 bar	1492 s	1142 s
3rd	84.1 bar	132 bar	85 bar	1375 s	1267 s
4th	149.1 bar	221 bar	130 bar	1264 s	1204 s
5th	219.3 bar	333 bar	202 bar	1230 s	1212 s

Table 18: Coupling results table

The average cycle period varies from 1500 to 1100 seconds, which is higher but close enough to the real working conditions (700-800 sec). The average cycle period drops as the pressure increases, due to the higher pressure difference which is the driving force for the coupling process and increases the kinetics of the reactions that take place.

The dehydrogenation time for second coupling is bigger than the expected one and the hydrogenation time is much smaller. This is probably because of inaccurate values of enthalpy and entropy that was used by the hydrogenating material which also explains the low temperature increase. Generally, the temperature profile of the hydrogenating processes in every coupling pair, was low. This is due to the delay of the time that hydrogen needs to escape from the dehydrogenating material to the stage that it is eventually adsorbed by the hydrogenating material.

The fraction profiles of hydrogenation and dehydrogenation or every coupling procedure have a relative slow beginning. In reality, they should be increased more rapidly in the beginning and slowing down when reaching the end of the process. This might be because of the initial plateau pressures that were calculated by the experimental data. Another potential explanation could be the activation energy values that are used in the simulation and they have the same value of 25k J/mol. The reason of selecting the same value was the lack of the required experimental data for calculating these values. Finally, the Enthalpy and Entropy of the materials are not fully constant and depend (albeit slightly) on thermodynamic properties. The deviation of these values will certainly affect plateau pressure so the reaction kinetics will be also affected.

1st coupling pair: LN603-2 (des) – T9 (ads)

The results of the pressure, the dehydrogenation/hydrogenation fraction and the temperature of the first coupling pair, are presented in Figure 36. The results behave physically in all the examined parameters. A comparison, of the pressure results of the numerical study with the experimental data on Figure 17, shows that they are quite similar in the pressure values to the operating pressure, on these stages, which is about 20 bar.

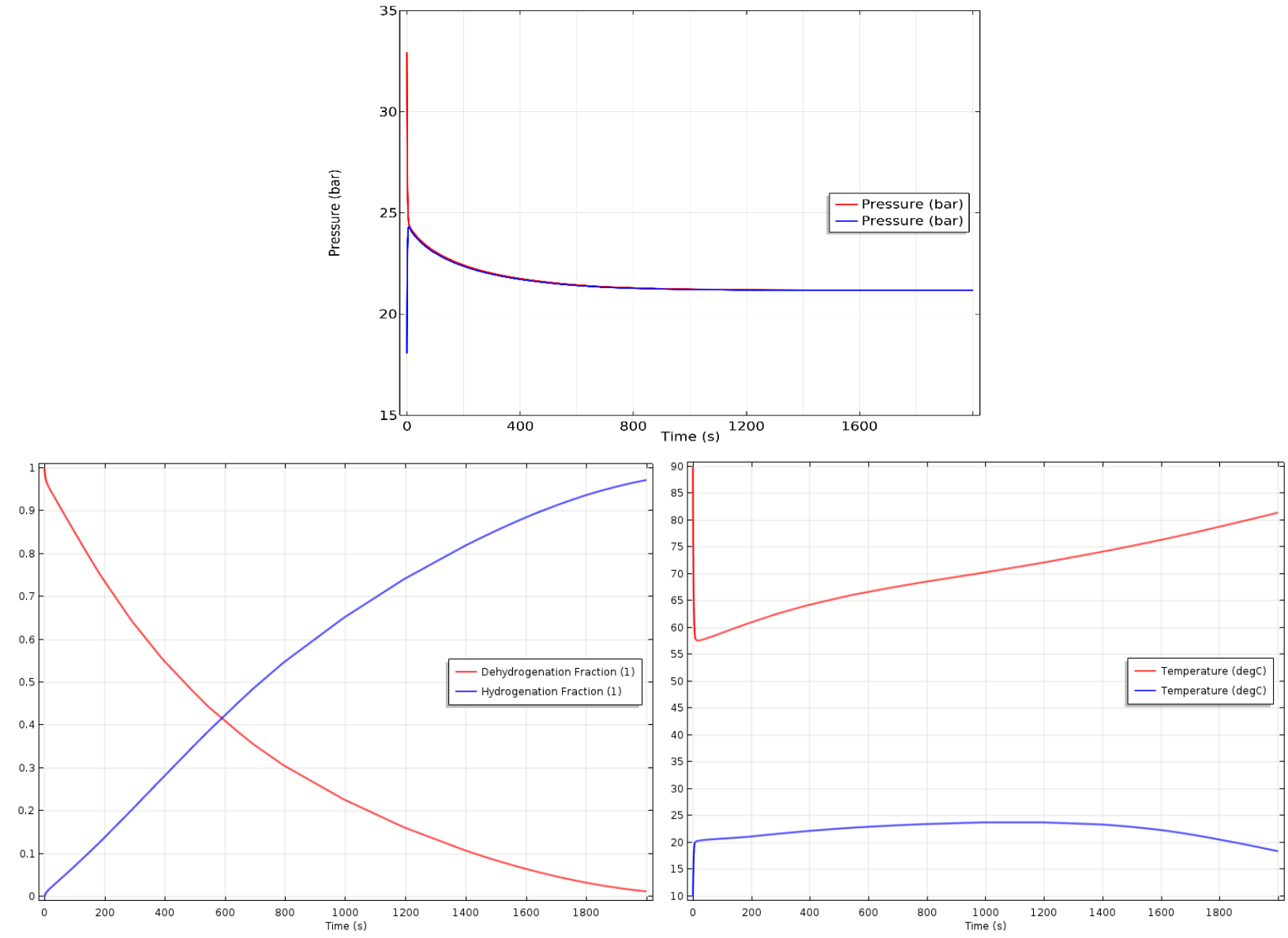

Figure 36: Pressure, Temperature and Hydrogenation/Dehydrogenation graphs for first coupling pair

2nd coupling pair: T9 (des) – T3 (ads)

In Figure 37, the results of the second coupling pair, are presented. The numerical results of Pressure are relatively close to the experimental data of the operating pressure of the same pair on Figure 17, which is about 50 bar. The hydrogenation time, in this pair, between 10% and 90% of hydrogenation fraction, is shorter than it was expected and it is due to not exact values of Enthalpy and Entropy that was inaccurate calculated from PCT data. This is also the reason why temperature behavior of hydrogenating stage (blue line) has smaller values than it was expected.

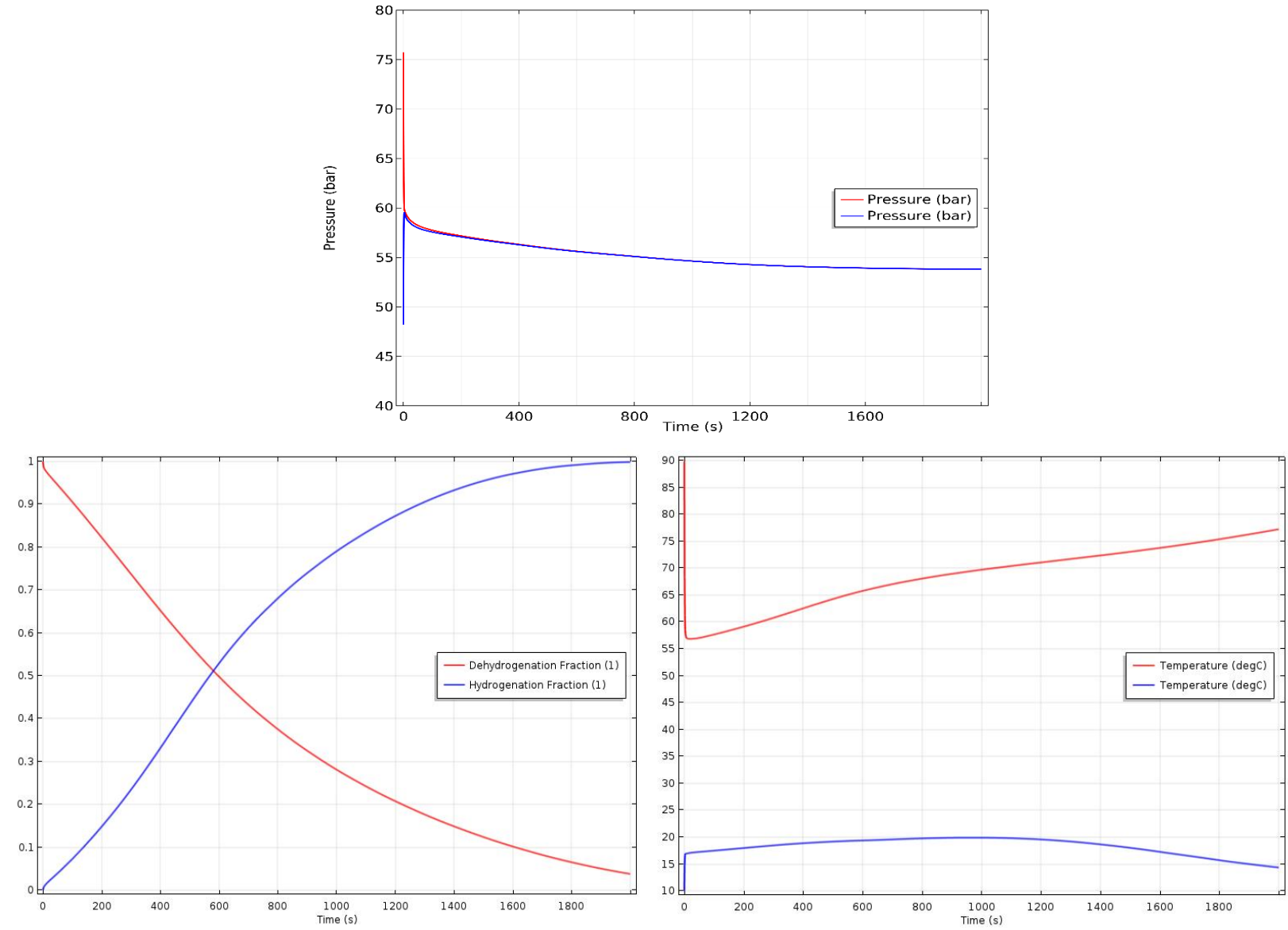

Figure 37: Pressure, Temperature and Hydrogenation/Dehydrogenation graphs for second coupling pair

3rd coupling pair: T3 (des) – T11 (ads)

The results of the 3rd coupling pair are shown in Figure 38. There is a good physical behavior of all the examined parameters. The pressure values of the numerical results show higher values in comparison to the experimental data of Figure 17. This is because of the luck of experimental data from the PCT curves for high temperatures, and probably a mismatch on the calculated values of Enthalpy and Entropy that were used, and they affect the value of plateau pressure.

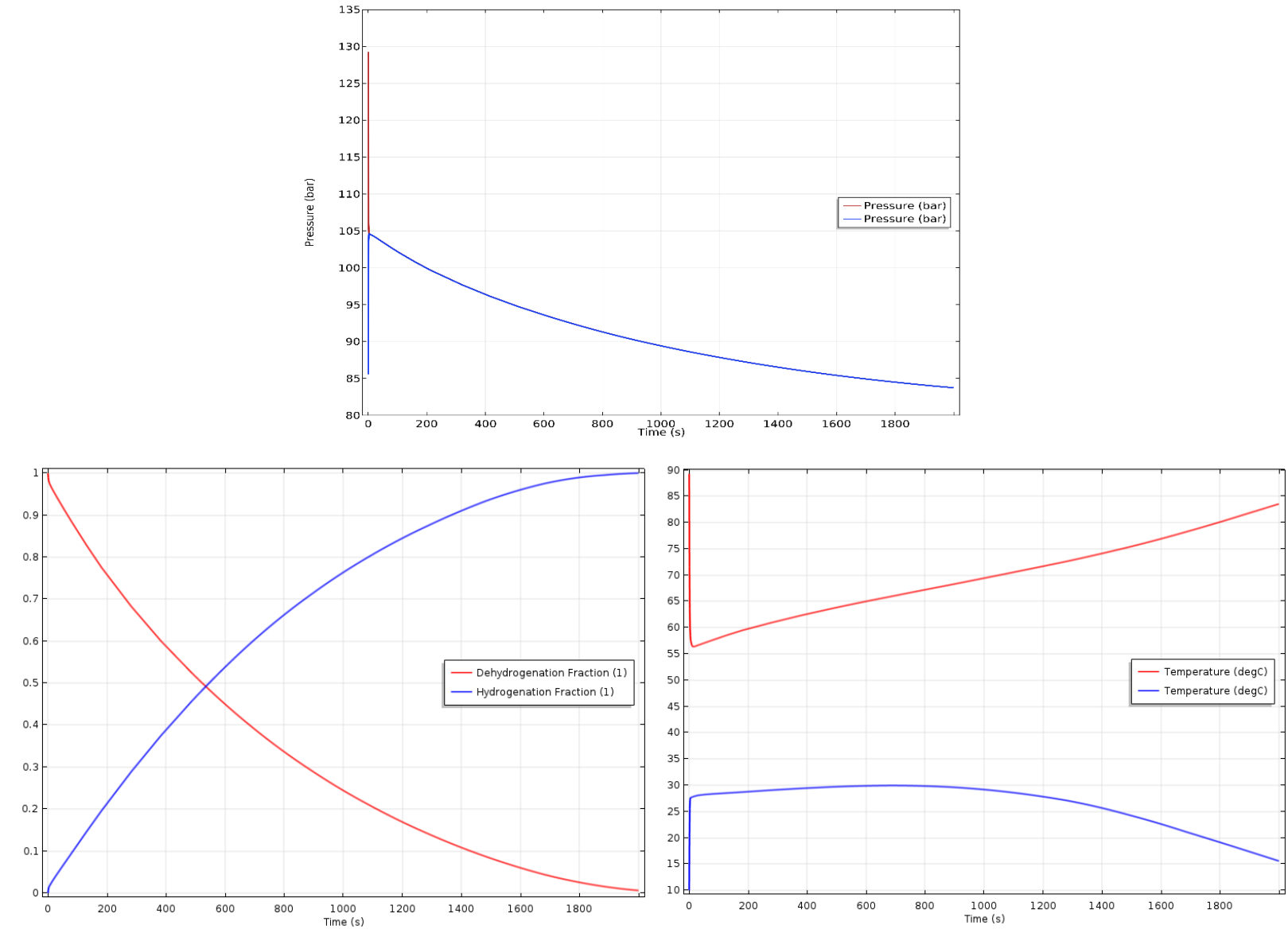

Figure 38: Pressure, Temperature and Hydrogenation/Dehydrogenation graphs for third coupling pair

4th coupling pair: T11 (des) – VF26 (ads)

The results of pressure, dehydrogenation/hydrogenation fraction and temperature for the 4th coupling pair, are presented in Figure 39. Once more, higher values of pressure are observed in comparison to the experimental data of Figure 17. This is due to the inaccuracy on the calculation of the Entropy and Enthalpy from the experimental data of PCT curves for high temperatures. It is also clear, that the hydrogenation and dehydrogenation time is shorter than the previous pairs. This is because of higher pressure deference that exists and consequently this increases the kinetics of both reactions.

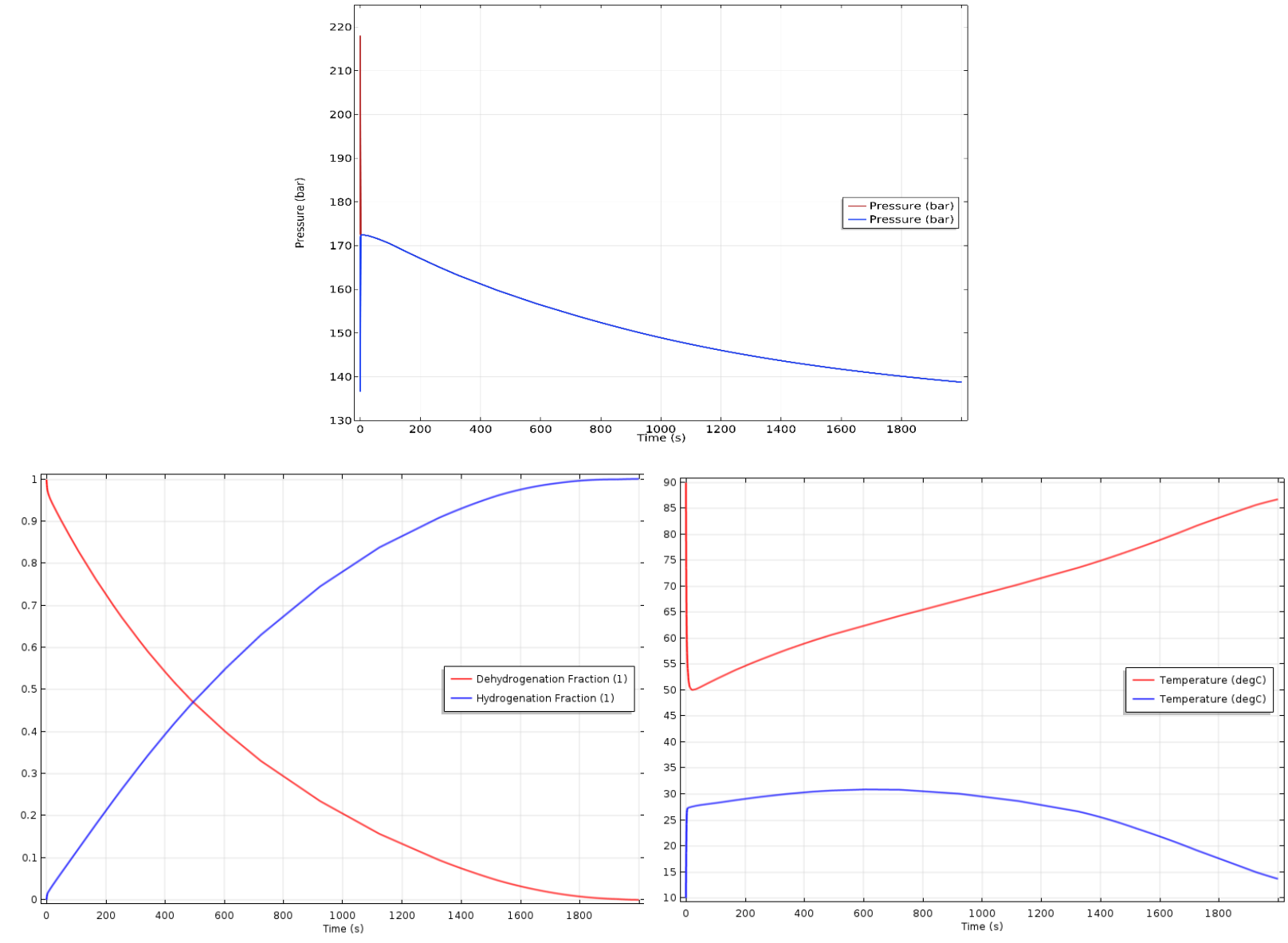

Figure 39: Pressure, Temperature and Hydrogenation/Dehydrogenation graphs for forth coupling pair

5th coupling pair: V26 (des) – VF28 (ads)

In Figure 40, the results of the 5th coupling pair that was investigated, are presented. Similar to the 3rd and the 4th coupling pairs the pressure behavior shows higher values than the experimental data of the operating pressure of Figure 17. This is due to the same reasons that had already described above. A shorter hydrogenation and dehydrogenation time is also observed here and this is due to the higher pressure difference that exist in these stages. This higher pressure difference affects the kinetics of both reactions, which lead to a shorter completion time for these processes.

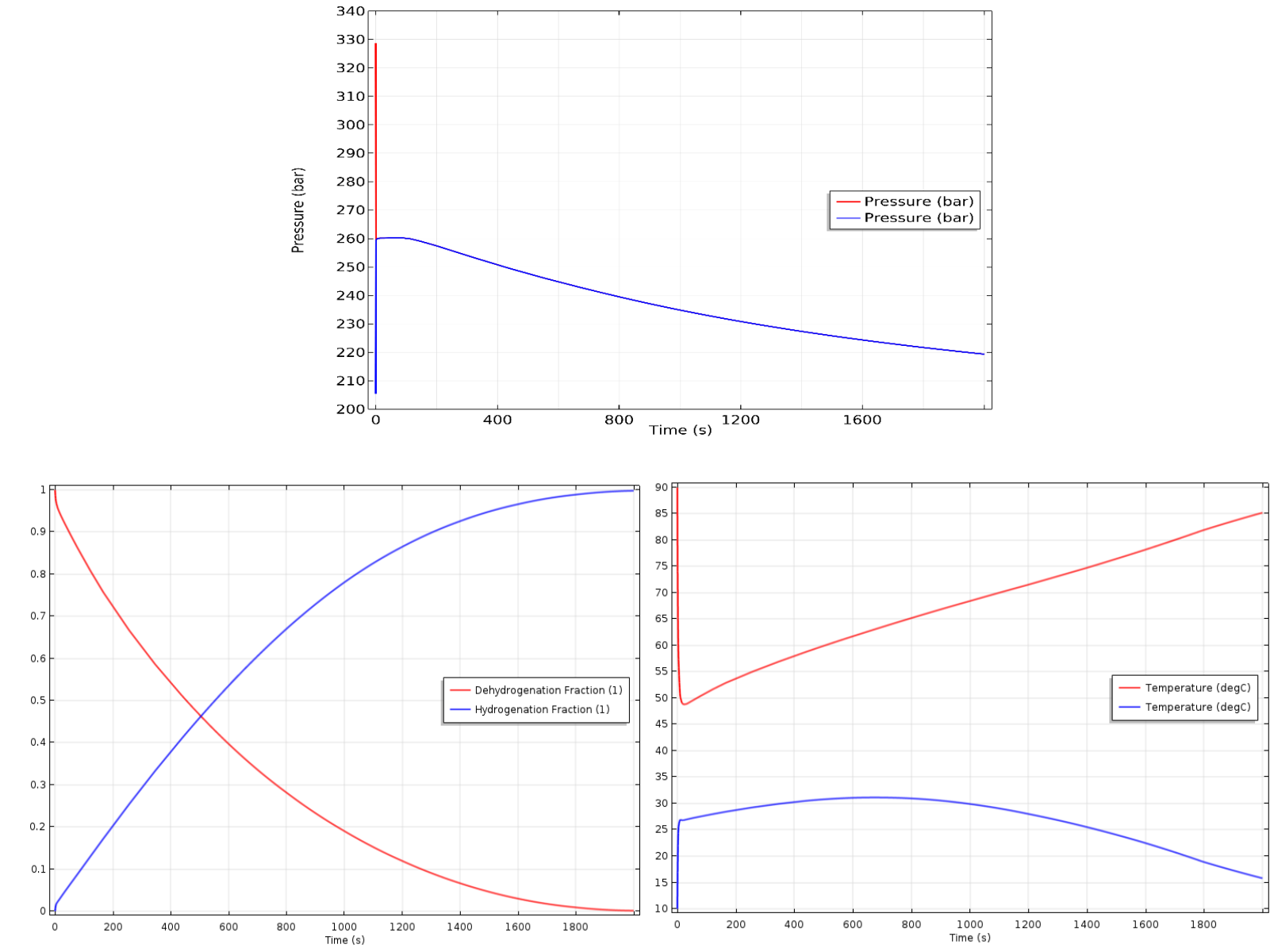

Figure 40: Pressure, Temperature and Hydrogenation/Dehydrogenation graphs for fifth coupling pair

In short, the results of the numerical analysis of the coupled hydrogenation and dehydrogenation process that take place during the operation of a MHC show a sound and physical behavior, in general. Some small undesired variations of the results are due to uncertainties on the selected values of the materials' properties.

More precise results on pressure behavior could be obtained through a better delineation of the thermodynamic behavior of these materials. Specifically, Plateau pressure, where Enthalpy and Entropy are engaged, could be better described through modeling of the variation of these properties, but this requires further experimental data of the materials.

Reactions kinetics is the most crucial factor for hydrogenation and dehydrogenation reactions which are, consequently, the most important results of the numerical investigation on the performance of this system. Reactions kinetics not only describes the behavior of hydrogen desorption and adsorption reactions, that must be fulfilled in logical time periods, but also are bonded with pressure and thermal behavior of this system. Once more, Enthalpy and Entropy are critical parameters at this stage due to the dependency of the reaction kinetics to the Equilibrium pressure. More than this, the kinetic constants C_d and C_a are factors that affect the reaction kinetics. Further investigation on experimental data is required for the selection of the right values of these constants as these are unique properties of the materials.

Furthermore, the level of accuracy on the simulation of the thermal behavior of the metal hydride compression system is of utmost importance. Metal hydride compressors are thermally driven machines, a fact that stresses two crucial things. Firstly, as described above, the precision on modeling the behavior of the reactions of hydrogenation and dehydrogenation, which generate and remove heat, respectively from their surrounding environment, where the critical factors are Entropy, Enthalpy and Activation energy. Secondly, due to the reason that this thermal driven operation is achieved through a heating and cooling medium, the effect of these heating and cooling flows and processes must be taken under closer consideration upon numerical modeling of these systems. Hence, all heat transfer related phenomena should be accounted for and integrated in the numerical analysis of these systems.

Conclusions

In this study, the numerical modeling of the coupled dehydrogenation – hydrogenation process, that takes place during the operation of a metal hydride compressor, was performed. The results demonstrate physically sound behavior of pressure, temperature, hydrogenation and dehydrogenation characteristics of these processes. Based on that, a numerical investigation of the operation behavior of a 6-stage metal hydride compressor was undertaken leading to a better understanding of the relevant processes.

In addition, useful conclusions were drawn regarding the numerical modeling of these processes. Highlighting the most important among them is the precise determination of the properties of the materials such as Enthalpy, Entropy, Activation energy and kinetics constants. Moreover, the need for including in the numerical modeling of the complete heat transfer interaction and effects from the cooling/heating medium, was indicated.

From the experience that was obtained through this study, the following suggestions for next steps are proposed. An extensive mapping of plateau pressures of the materials, at several temperature levels in the operating temperature range of a MHC, through PCT experimental data, would be very important for modeling the thermodynamic and kinetics properties with high precision. This will diminish various uncertainties regarding the interaction of the pressure, the temperature and the reaction behavior that are related to the material properties. Furthermore, incorporating the numerical modeling of the cooling/heating media flows, in a computational-inexpensive way, will offer more accuracy towards the real operation conditions of a Metal hydride compressor.

Bibliography

1. *New approaches to hydrogen storage.* Graetz J. s.l. : Chem. Soc. Rev., 2009, Vols. 38, p:73-82. DOI: 10.1039/B718842K.

2. *A comprehensive review on PEM water electrolysis.* Carmo M., et al. 12, p:4901-4934, s.l. : Int. J. Hydrogen Energy, 2013, Vol. 38. DOI: 10.1016/j.ijhydene.2013.01.151.

3. *Wind energy and the hydrogen economy—review of the technology.* Sherif S., Barbir F. and Veziroglu T. 5, s.l. : Solar Energy, 2005, Vol. 78. DOI: 10.1016/j.solener.2005.01.002.

4. *Hydrogen storage methods.* Zuttel A. 4, p:157-172, s.l. : The Science of Nature, 2004, Vol. 91. DOI: 10.1007/s00114-004-0516-x.

5. Amos W. A. *Costs of Storing and Transporting Hydrogen.* s.l. : National Renewable Energy Lab (US), 1999. DOI: 10.2172/6574.

6. Bloch H. P. and Hoefner J. J. *Reciprocating Compressors: Operation and Maintenance (1st).* s.l. : Gulf Professional Publishing, 1996. ISBN: 9780884155256.

7. Pahwa P. K. and Pahwa G. K. *Hydrogen Economy.* s.l. : The Energy and Resources Institute (TERI), 2014. ISBN: 8179935043.

8. *Heat transfer analysis of liquid piston compressor for hydrogen applications.* Kermani N. A. 35, p: 11522-11529, s.l. : Int. J. Hydrogen Energy, 2015, Vol. 40. DOI: 10.1016/j.ijhydene.2015.01.098.

9. *Comparison of heat transfer models for reciprocating compressor.* Tuhovcak J., Hejcik J. and Jicha M. 25, p: 607-615, s.l. : Applied Thermal Engineering, 2016, Vol. 103. DOI: 10.1016/j.applthermaleng.2016.04.120.

10. *Experimental and Numerical Study of Snuber in Hydrogen Compressor.* Shiddiqur Rahman M. 2, p: 21-25, s.l. : Int. J. Sci. Eng, 2012, Vol. 3. ISSN: 2086-5023.

11. *Design Considerations for High-Pressure Reciprocating Compressors for Refinery Services.* Dwivedi S. N. s.l. : International Compressor Engineering Conference, 1990. https://docs.lib.purdue.edu/icec/715.

12. *Increase reliability of reciprocating hydrogen compressors.* Leonard S. M. 1, s.l. : Hydrocarbon Processing, 1996, Vol. 75. OSTI: 178356.

13. Ahmed S. and Sutherland E. *Hydrogen Compression, Storage, and Dispensing Cost Reduction Workshop Final Report.* s.l. : DOE's Argonne National Laboratory, 2013. https://www.energy.gov/sites/prod/files/2014/03/f9/2013_csd_workshop_report.pdf.

14. Brown R. N. *Compressors: Selection and Sizing (2nd).* s.l. : Gulf Professional Publishing, 1997. ISBN: 0884151646.

15. Bloch H. P. *A Practical Guide to Compressor Technology (2nd).* s.l. : John Wiley & Sons, 2006, 2006. ISBN: 0471929522.

16. *Comparison of electrical energy efficiency of atmospheric and high-pressure electrolysers.* Roy A., Watson S. and Infield D. 14, p: 1964-1979, s.l. : Int. J. Hydrogen Energy, 2006, Vol. 31. DOI: 10.1016/j.ijhydene.2006.01.018.

17. McKetta J. J. *Encyclopedia of Chemical Processing and Design.* s.l. : CRC Press, 1998. ISBN: 0824726154.

18. Stolten D. *Hydrogen and Fuel Cells: Fundamentals, Technologies and Applications.* s.l. : John Wiley & Sons, 2010. ISBN: 3527327118.

19. *A review of linear compressors for refrigeration.* Liang K. p: 253-273, s.l. : Int. J. Refrigeration, 2017, Vol. 84. DOI: 10.1016/j.ijrefrig.2017.08.015.

20. Broerman E. L., et al. *Hydrogen Compression Application of the Linear Motor Reciprocating Compressor (LMRC).* s.l. : Southwest Research Institute, 2015. https://www.hydrogen.energy.gov/pdfs/progress15/iii_7_broerman_2015.pdf.

21. Scott R. B., Denton W. H. and Nicholls C. M. *Technology and Uses of Liquid Hydrogen (1st).* s.l. : Elsevier, 1964. DOI: 10.1016/C2013-0-01825-7.

22. *Theoretical and experimental investigations on the partial scaling method for the Oxford-type moving-coil linear compressor.* Zhang L., et al. p: 26-35, s.l. : Cryogenics, 2015, Vol. 69. DOI: 10.1016/j.cryogenics.2015.03.004.

23. *Linear Compressors for Clean and Specialty Gases.* Unger R. L. s.l. : International Compressor Enngineering Conference, 1998. https://docs.lib.purdue.edu/cgi/viewcontent.cgi?article=2214&context=icec.

24. *Modeling and Analysis of Deformation on a Flexible Bearing in Linear Compressor .* Sivareddy V. V. 1, s.l. : Int. J. Mech. Eng., 2014, Vol. 3. ISSN: 2278 – 0149.

25. *A comprehensive model of a miniature-scale linear compressor for electronics cooling.* Bradshaw C. R., Groll E. A. and Garimela S. V. 1, p: 63-73, s.l. : Int. J. Refrigeration, 2011, Vol. 34. DOI: 10.1016/j.ijrefrig.2010.09.016.

26. *Quasi-Izothermal Compressors And Expanders With Liquid Piston.* Torok A., et al. s.l. : Termotehnica, 2013. HAL: hal-02461111.

27. *Liquid piston gas compression.* Van de Ven J. D. and Li P. Y. 10, p: 2183-2191, s.l. : Applied Energy, 2009, Vol. 86. DOI: 10.1016/j.apenergy.2008.12.001.

28. *A Hybrid Energy Storage System Based on Compressed Air and Supercapacitors With Maximum Efficiency Point Tracking.* Lemofouet S. and Rufer A. 4, p: 1105-1115, s.l. : IEEE Transactions on Industrial Electronics, 2006, Vol. 53. DOI: 10.1109/TIE.2006.878323.

29. *A review of compressed-air energy storage.* Yu Q., et al. s.l. : Journal of Renewable and Sustainable Energy, 2019, Vol. 11. DOI: 10.1063/1.5095969.

30. Lyons W. C., et al. *Air and Gas Drilling Manual - Applications for Oil and Gas Recovery Wells and Geothermal Fluids Recovery Wells (3rd).* s.l. : Gulf Professional Publishing, 2009. DOI: 10.1016/B978-0-12-370895-3.X0001-6.

31. Forsthoffer W. E. *Forsthoffer's Best Practice Handbook for Rotating Machinery.* s.l. : Elsevier, 2011. ISBN: 0080966772.

32. Liptak B. G. *Instrument Engineers' Handbook, Volume One: Process Measurement and Analysis.* s.l. : CRC Press, 2003. ISBN: 1420064029.

33. *Understanding Ionic Liquids at the Molecular Level: Facts, Problems, and Controversies.* Weingartner H. 4, s.l. : Angewandte Chemie International Edition, 2008, Vol. 47. DOI: 10.1002/anie.200604951.

34. *Ionic Liquids as Operating Fluids in High Pressure Applications.* Predel T. and Schlucker E. 11, s.l. : Chemical Engineering & Technology, 2007, Vol. 30. 10.1002/ceat.200700276.

35. *Gas Solubility in Ionic Liquids.* Lei Z., Dai C. and Chen B. 2, p: 1289–1326, s.l. : Chemical Reviews, 2014, Vol. 114. DOI: 10.1021/cr300497a.

36. *From prototype to serial production - manufacturing hydrogen fuuelling stations.* Mayer M. s.l. : A3PS Conference, 2014. http://www.a3ps.at/sites/default/files/conferences/2014/papers/01_linde_mayer.pdf.

37. Robert M. and Wical B. *Total Energy Independence for the United States: A Twelve-Year Plan.* s.l. : iUniverse, 2007. ISBN: 059543519X.

38. *Electrochemical hydrogen compressor.* Rohland B., et al. 24, p: 3841-3846, s.l. : Electrochimica Acta, 1998, Vol. 43. DOI: 10.1016/S0013-4686(98)00144-3.

39. *A comparative analysis of the cryo-compression and cryo-adsorption hydrogen storage methods.* G., Petitpas, et al. 20, p: 10564-10584, s.l. : Int. J. Hydrogen Energy, 2014, Vol. 39. DOI: 10.1016/j.ijhydene.2014.04.200.

40. *The Cryogenic Hydrogen Compressor System.* s.l. : Air Products. http://www.airproducts.in/~/media/downloads/h/hydrogen-support-microsite/en-cryogenic-hydrogen-compressor-system.pdf?la=kn-IN.

41. *Insulated pressure vessels for hydrogen storage on vehicles.* Aceves S. M., Berry G. D. and Rambach G. D. 7, p: 583-591, s.l. : Int. J. Hydrogen Energy, 1998, Vol. 23. DOI: 10.1016/S0360-3199(97)00079-7.

42. *Technical assessment of cryo-compressed hydrogen storage tank systems for automotive applications.* Ahluwalia R. K., et al. 9, p: 4171-4184, s.l. : Int. J. Hydrogen Energy, 2010, Vol. 35. DOI: 10.1016/j.ijhydene.2010.02.074.

43. Grasman S. E. *Hydrogen Energy and Vehicle Systems.* s.l. : CRC Press, 2012. ISBN: 1439826811.

44. *Safe, long range, inexpensive and rapidly refuelable hydrogen vehicles with cryogenic pressure vessels.* Aceves S. M., et al. 5, p: 2480-2489, s.l. : Int. J. Hydrogen Energy, 2013, Vol. 38. DOI: 10.1016/j.ijhydene.2012.11.123.

45. *The compression of hydrogen in an electrochemical cell based on a PE fuel cell design.* Strobel R., et al. 2, p: 208-215, s.l. : Journal of Power Sources, 2002, Vol. 105. DOI: 10.1016/S0378-7753(01)00941-7.

46. *Electrochemical Hydrogen Compression.* Bouwman P. J., et al. 3, s.l. : The Electrochemical Society, 2014, Vol. 64. DOI: 10.1149/06403.1009ecst.

47. *Advances in Electrochemical Compression of Hydrogen.* M., Moton J., Jammes B. and Colella G. s.l. : International Conference on Fuel Cell Science, Engineering and Technology, 2014. DOI: 10.1115/FuelCell2014-6641.

48. Stolten D. *Hydrogen and Fuel Cells: Fundamentals, Technologies and Applications.* s.l. : John Wiley & Sons, 2010. ISBN: 3527327118.

49. *Electrochemical compressor driven metal hydride heat pump.* Y., Tao, et al. p: 278-288, s.l. : International Journal of Refrigeration, 2015, Vol. 60. 10.1016/j.ijrefrig.2015.08.018.

50. *Separation and compression characteristics of hydrogen by use of proton exchange membrane.* K., Onda, et al. 1, p: 1-8, s.l. : Journal of Power Sources, 2007, Vol. 164. 10.1016/j.jpowsour.2006.10.018.

51. *Thermodynamics of thermally-driven adsorption compression.* Santori G. and Luberti M. p: 1-9, s.l. : Sustainable Materials and Technologies, 2016, Vol. 10. 10.1016/j.susmat.2016.09.001.

52. *Low-pressure adsorption storage of hydrogenLow-pressure adsorption storage of hydrogen.* Chahine R. and Bose T. K. 2, p: 161-164, s.l. : Int. J. Hydrogen Energy, 1994, Vol. 19. DOI: 10.1016/0360-3199(94)90121-X.

53. *Heat and Mass Transfer in Solid State Hydrogen Storage: A Review.* Murthy S. S. 3, s.l. : J. Heat Transfer, 2012, Vol. 134. DOI: 10.1115/1.4005156.

54. *Metal hydride hydrogen compressors: A review.* Lototsky M.V., et al. 11, p: 5818-5851, s.l. : Int. J. Hydrogen Energy, 2014, Vol. 39. DOI: 10.1016/j.ijhydene.2014.01.158.

55. *Hydride alloys properties investigations for hydrogen sorption compressor.* Dehouche Z., Grimard N. and Laurencellle F. 1-2, p: 224-236, s.l. : J. Alloyw and Compounds, 2005, Vol. 399. DOI: 10.1016/j.jallcom.2005.01.029.

56. *Performance tests on a thermally operated hydrogen compressor.* Muthukumar P., Maiya M. P. and Murthy S. S. 1, p: 463-469, s.l. : Int. J. Hydrogen Energy, 2008, Vol. 33. DOI: 10.1016/j.ijhydene.2007.07.019Get.

57. Koultoukis D. E., et al. Two-Stage Hydrogen Compression Using Zr-Based Metal Hydrides. *Solid State Phenomena.* 2012, Vols. 194, p: 249-253, DOI: 10.4028/www.scientific.net/SSP.194.249.

58. *High-temperature activated AB2 nanopowders for metal hydride hydrogen compression.* Koultoukis E. D., et al. 4, s.l. : International Journal of Energy Research, 2014, Vol. 38. DOI:10.1002/er.3147.

59. *Parametric studies on a metal hydride based single stage hydrogen compressor.* P., Muthukumar, M., Prakash and S., Murthy S. 10, p: 1083-1092, s.l. : Int. J Hydrogen Energy, 2002, Vol. 27. DOI: 10.1016/S0360-3199(02)00005-8.

60. *Heat and mass transfer in metal hydride reaction beds: Experimental and theoretical results.* Mayer U., Groll M. and Supper W. 1-2, p: 235-244, s.l. : Journal of the Less Common Metals, 1987, Vol. 131. DOI: 10.1016/0022-5088(87)90523-6.

61. *Heat and mass transfer in metal hydride beds for heat pump applications.* Choi H. and Mills A. F. 6, p:1281-1288, s.l. : Int. J. Heat and Mass Transfer, 1990, Vol. 33. DOI: 10.1016/0017-9310(90)90257-U.

62. *Heat and mass transfer models in metal-hydrogen reactor.* Nasrallah S. B. and Jemni A. 1, p: 67-76, s.l. : Int. J. Hydrogen Energy, 1997, Vol. 22. DOI: 10.1016/S0360-3199(96)00039-0.

63. *Experimental and theoretical study of ametal–hydrogen reactor.* Jemni A., Nasrallah S. B. and Lamloumi J. 7, p: 631-644, s.l. : Int. J. Hydrogen Energy, 1999, Vol. 24. DOI: 10.1016/S0360-3199(98)00117-7.

64. *Prediction of transient heat and mass transfer in a closed metal–hydrogen reactor.* Askri F., Jemni A. and Nasrallah S. B. 2, p:195-208, s.l. : Int. J. Hydrogen Energy, 2004, Vol. 29. DOI: 10.1016/S0360-3199(03)00089-2.

65. *A new algorithm for solving transient heat and mass transfer in metal–hydrogen reactor.* Askri F., Salah M. B. and Nasrallah S. B. 19, p: 8315-8321, s.l. : Int. J. Hydrogen Energy, 2009, Vol. 34. DOI: 10.1016/j.ijhydene.2009.07.072.

66. *Optimization of hydrogen storage in metal-hydride tanks.* F., Askri, et al. 2, p:897-905, s.l. : Int. J. Hydrogen Eergy, 2009, Vol. 34. DOI: 10.1016/j.ijhydene.2008.11.021\.

67. *Parametric studies on a metal-hydride cooling system.* Mellouli S., et al. 9, p:3945-3952, s.l. : Int. J. Hydrogen Energy, 2009, Vol. 34. DOI: 0.1016/j.ijhydene.2009.03.010.

68. *Numerical simulation of heat and mass transfer in metal hydride hydrogen storage tanks for fuel cell vehicles.* Mellouli S., et al. 4, p:1693-1705, s.l. : Int. J. Hydrogen Eergy, 2010, Vol. 35. DOI: 10.1016/j.ijhydene.2009.12.052.

69. *Parametric studies on a metal hydride based hydrogen storage device.* Muthukumar P. and Dewan A. 18, p: 4988-4997, s.l. : Int. J. Hydrogen Energy, 2007, Vol. 32. DOI: 10.1016/j.ijhydene.2007.08.010.

70. *Numerical simulation of coupled heat and mass transfer in metal hydride-based hydrogen storage reactor.* Muthukumar P. and Ramana S. V. 1-2, p: 466-472, s.l. : J. Alloys ad Compounds, 2009, Vol. 472. DOI: 10.1016/j.jallcom.2008.04.088.

71. *Hierarchical methodology for modeling hydrogen storage systems. Part I: Scoping models.* Bruce J. and Anton D. L. 5, p:2269-2277, s.l. : Int. J. Hydrogen Energy, 2009, Vol. 34. DOI: 10.1016/j.ijhydene.2008.12.070.

72. *Hierarchical methodology for modeling hydrogen storage systems. Part II: Detailed models.* Bruce J. and Anton D. L. 7, p:2992-3004, s.l. : Innt. J. Hydrogen Energy, 2009, Vol. 34. DOI: 0.1016/j.ijhydene.2008.12.056.

73. *Optimization of internal heat exchangers for hydrogen storage tanks utilizing metal hydrides.* L., Garrisson. S., J., Hardy B. and C., Corgnale. 2, p: 2850-2861, s.l. : Int. J. Hydrogen Energy, 2012, Vol. 377. DOI: 0.1016/j.ijhydene.2011.07.044.

74. *Identifying heat and mass transfer characteristics of metal hydride reactor during adsorption—Parameter analysis and numerical study.* Yang F., et al. 3, p:1014-1022, s.l. : Int. J. Hydrogen Energy, 2008, Vol. 33. DOI: 10.1016/j.ijhydene.2007.11.007.

75. *An optimization study on the finned tube heat exchanger used in hydride hydrogen storage system – analytical method and numerical simulation.* Nyamsi S. N., Yang F. and Zhang Z. 21, p: 16078-16092, s.l. : Int. J. Hydrogen Energy, 2012, Vol. 37. DOI: 10.1016/j.ijhydene.2012.08.074.

76. *System simulation modeling and heat transfer in sodium alanate based hydrogen storage systems.* Raju M. and Kumar S. 2, p: 1578-1591, s.l. : Int. J. Hydrogen Energy, 2011, Vol. 36. DOI: 10.1016/j.ijhydene.2010.10.100.

77. *Optimization of heat exchanger designs in metal hydride based hydrogen storage systems.* Raju M. and Kumar S. 3, p: 2767-2778, s.l. : Int. J. Hydrogen Energy, 2012, Vol. 37. DOI: 10.1016/j.ijhydene.2011.06.120.

78. *Numerical simulation of sorption/desorption processes in metal-hydride systems for hydrogen storage and purification. Part I: Development of a mathematical model.* Minko K. B., Artemov V. I. and Yankov G. G. p: 683-692, s.l. : Int. J. Hydrogen Energy, 2014, Vol. 68. DOI: 10.1016/j.ijheatmasstransfer.2013.09.056.

79. *Numerical simulation of sorption/desorption processes in metal-hydride systems for hydrogen storage and purification. Part II: Verification of the mathematical model.* Minko K. B., Artemov V. I. and Yanjkov G. G. p: 693-702, s.l. : Int. J. Hydrogen Energy, 2014, Vol. 68. DOI: 10.1016/j.ijheatmasstransfer.2013.09.057.

80. *Simulation study on the outlet flow dynamics of a hydride-based hydrogen storage canister for medical use.* Yang F., et al. 12, p: 6548-6557, s.l. : Int. J. Hydrogen Energy, 2014, Vol. 39. DOI: 10.1016/j.ijhydene.2014.02.048.

81. *Metal hydride hydrogen compression: recent advances and future prospects.* Yartis V., et al. s.l. : Applied Physics A, 2016, Vol. 122. DOI: 10.1007/s00339-016-9863-7.

82. *Modelling of phase equilibria in metal–hydrogen systems.* Lototskyy M. V., Yartys V. A. and Marinin V. S. 11, p: 27-31, s.l. : Journal of Alloys and Compounds , 2003, Vols. 356-357. DOI: 10.1016/S0925-8388(03)00095-1.